

# **Regioisomeric BODIPY- Benzodithiophene Dyads and Triads with Multiple Emissions as Viscosity and Temperature Sensors**

**ASWATHY P.R.**

*A dissertation submitted for the partial fulfilment  
of BS-MS dual degree in science.*



**Indian Institute of Science Education and Research, Mohali**

**April 2019**

# Certificate of Examination

This is to certify that the dissertation titled “**Regioisomeric BODIPY-Benzodithiophene Dyads and Triads with Multiple Emissions as Viscosity and Temperature Sensors**” submitted by Ms. Aswathy P. R. (Reg. No. MS14160) for the partial fulfillment of BS-MS dual degree programme of the Institute, has been examined by the thesis committee duly appointed by the Institute. The committee finds the work done by the candidate satisfactory and recommends that the report be accepted.

Dr. Sugumar Venkataramani

Assistant Professor

IISER Mohali

Dr. Raj Kumar Roy

Assistant Professor

IISER Mohali

Dr. Sanchita Sengupta

Assistant Professor

IISER Mohali

(Supervisor)

Dated : April , 2019

# Declaration

The work presented in this dissertation has been carried out by me under the guidance of Dr. Sanchita Sengupta at the Indian Institute of Science Education and Research Mohali.

This work has not been submitted in part or in full for a degree, a diploma, or a fellowship to any other university or institute. Whenever contributions of others are involved, every effort is made to indicate this clearly, with due acknowledgement of collaborative research and discussions. This thesis is a bonafide record of original work done by me and all sources listed within have been detailed in the bibliography.

Aswathy P. R.

(Candidate)

Dated: April , 2019

In my capacity as the supervisor of the candidate's project work, I certify that the above statements by the candidate are true to the best of my knowledge.

Dr. Sanchita Sengupta

(Supervisor)

# Acknowledgement

I want to express my deepest thanks to my guide Dr. Sanchita Sengupta for the support and help she gave me towards the completion of this project. She corrected me when I was wrong and gave me comments which are helpful for the progress of the project.

I wish to thank my committee members Dr. Sugumar Venkataramani and Dr. Raj Kumar Roy for giving valuable suggestions and questions.

I would like to express my thanks to professor S. Arulananda Babu for introducing me to organic chemistry and giving opportunity for working in his lab with Dr. Gowri and for helping me to learn all the techniques related to organic chemistry. And a special thanks to Dr. Ramesh Ramachandran for motivating me to take chemistry as my major.

Thanks a lot to my lab members Narendra, Sushil and Kavita for their help, support and immense knowledge sharing. Thanks for keeping motivated and providing a friendly atmosphere.

I would also like to thank RKR group members Arjun, Deepak and Umer for their help, support and maintaining a cheerful and comfortable atmosphere.

And thanks to all of my friends who were there for help and motivation. Thanks to Bella, Adheena, Aswathy, Arya, Vinita, Asha, Vishnu, Akshay and Joyal for being there for me.

I would like to thank vidhya lakshmi, who was there for me in my good and bad times and thanks to shiny, swetha, sruthy for their late night classes.

A lot of thanks to my parents and my whole family for their love, care, trust, help, motivation, support and for everything they have given. I'm really blessed to have each one of them in my life.

# Contents

List of Figures.....	i
List of Tables.....	iii
List of Scheme.....	iv
List of Abbreviations.....	v
Abstract.....	1
Chapter 1 Introduction.....	2
Chapter 2 Result and Discussion.....	13
Chapter 3 Summary and Outlook.....	30
Chapter 4 Experimental Section.....	32
References.....	47
Appendix.....	49

# List of figures

**Figure. 1.1** BODIPY core

**Figure. 1.2** BDT core

**Figure. 1.3** Twisted Intramolecular Charge Transfer Dynamics.

**Figure. 1.4** Solvent effects on electronic state energies.

**Figure. 1.5** Solvatochromism in 4-dimethylamino-4'-nitrostilbene.

**Figure. 1.6** Aggregation-induced emission (AIE) in TPE.

**Figure. 1.7** Proposed Mechanism for TICT and AIE Processes in BODIPY Luminogens.

**Figure. 1.8** General chemical structure of fluorescent molecular rotors (FMRs) with its working principle.

**Figure. 1.9** Molecular structure and HOMO-LUMO calculations of **p-ADA**.

**Figure. 1.10** Optical properties of **p-ADA**.

**Figure. 1.11** Molecular Design principle of our work.

**Figure. 2.1** Optical properties of **BDP-p-Br** and **BDP-m-Br** in solution and thin film.

**Figure. 2.2** Orbital plots of HOMO and LUMO of **m-ADA**

**Figure. 2.3** Orbital plots of HOMO-LUMO of **m-AD**.

**Figure. 2.4** Orbital plots of HOMO-LUMO of **p-AD**.

**Figure. 2.5** Electronic absorption properties of dyads and triad.

**Figure. 2.6** Fluorescence emission spectra for **m-AD**, **p-AD**, **m-ADA**.

**Figure. 2.7** Fluorescence emission spectra of **p-AD** in solvents of different polarity and in different hexane/THF (v/v) solvent mixtures.

**Figure. 2.8** Solutions of fluorescence solvatochromism of **p-AD** in hexane/THF mixtures.

**Figure. 2.9** Fluorescence emission spectra of **m-ADA** and **m-AD** in different solvents.

**Figure. 2.10** Aggregate induced emission in **p-AD**, **m-ADA**, and **m-AD** in different mixture of water/THF mixture.

**Figure. 2.11** Solutions of **m-ADA** in THF/water showing AIE effect.

**Figure. 2.12** Emission spectra of **p-AD** and **m-ADA** in chloroform.

**Figure. 2.13** Emission spectra of **p-AD**, **m-ADA** and **m-AD** in toluene.

**Figure. 2.14** Emission spectra of **p-AD** in THF at different temperature and CIE

Chromaticity plot of **p-AD** in THF at different temperatures.

**Figure. 2.15** Emission spectra of **p-AD**, **m-ADA** and **m-AD** in solution of varying viscosities.

**Figure. 2.16** Temperature effect on a particular viscosity.

# List of tables

**Table 1** : Comparison of absorption and emission of BODIPYs in solution and thin films.

**Table 2** : Comparison of torsional angles and HOMO LUMO energy level of dyads and triads.

**Table 3** : Comparison of absorption and emission of dyads and triads.

**Table 4** : Summary of the work.



# List of schemes

**Scheme 2.1.** General scheme for synthesis of m-ADA, m-AD and p-AD.

**Scheme 4.1.** Synthesis of dipyrromethane (DPM)

**Scheme 4.2.** Synthesis of acceptor m-BODIPY-Br.

**Scheme 4.3.** Synthesis of acceptor p-BODIPY-Br.

**Scheme 4.4.** Synthesis of (*N,N*-diethyl)thiophenecarboxylamide.

**Scheme 4.5.** Synthesis of BDT-dione.

**Scheme 4.6.** Synthesis of alkylated Benzodithiophene.

**Scheme 4.7.** Synthesis of Donor.

**Scheme 4.8.** Stille coupling of acceptor and donor to form triad m-ADA.

**Scheme 4.9.** Synthesis of m-AD and p-AD compounds using Stille coupling.

**Scheme 4.10.** Synthesis of alkylated BDT with *n*-BuLi as base.

**Scheme 4.11.** Synthesis of 8-bis((2-ethylhexyl)oxy)benzo[1,2-*b*:4,5-*b'*]dithiophene.

**Scheme 4.12.** Synthesis of 8-bis((2-ethylhexyl)oxy)benzo[1,2-*b*:4,5-*b'*]dithiophene-2,6-diyl)bis(trimethylstannane).

**Scheme 4.13.** Synthesis of 8-bis((2-ethylhexyl)oxy)benzo[1,2-*b*:4,5-*b'*]dithiophene using a mild base  $K_2CO_3$ .

**Scheme 4.14.** Synthesis of 4,8-bis(triisopropylsilylethynyl)benzo[1,2-*b*:4,5-*b'*]dithiophene.

**Scheme 4.15.** Synthesis of benzo[1,2-*b*:4,5-*b'*]dithiophene-4,8-diol from benzo[1,2-*b*:4,5-*b'*]dithiophene-4,8-dione.

**Scheme 4.16.** Synthesis of 8-bis((2-ethylhexyl)oxy)benzo[1,2-*b*:4,5-*b'*]dithiophene using DMF as solvent.

**Scheme 4.17.** Synthesis of 4,8-Bis(trifluoromethanesulfonyloxy)benzo[1,2-*b*:4,5-*b'*]dithiophene.

**Scheme 4.18.** Synthesis of 4,8-di(oct-1-yn-1-yl)benzo[1,2-*b*:4,5-*b'*]dithiophene.

# Notations and abbreviations

BODIPY	-	Boradiazaindacene
BDT	-	Benzodithiophene
TICT	-	Twisted Intramolecular Charge Transfer
LE state	-	Locally Excited state
Tol	-	Toluene
AIE	-	Aggregate Induced Emission
OPV	-	Organic Photovoltaics
DDQ	-	2,3-Dichloro-5,6-dicyano-1,4-benzoquinone
m-ADA	-	meta-acceptor-donor-acceptor
m-AD	-	meta-acceptor-donor
p-AD	-	para-acceptor-donor
BDP-p-Br	-	Boradiazaindacene-para-Bromo
BDP-m-Br	-	Boradiazaindacene-meta-Bromo

DCM	-	Dichloromethane
C	-	Concentration
DFT	-	Density Functional Theory
HOMO	-	Highest occupied molecular orbital
LUMO	-	Lowest unoccupied molecular orbital
THF	-	Tetrahydrofuran
DMF	-	Dimethylformamide
CHCl <sub>3</sub>	-	Chloroform
CDCl <sub>3</sub>	-	Deuterated chloroform
K <sub>2</sub> CO <sub>3</sub>	-	Potassium Carbonate
NaHCO <sub>3</sub>	-	Sodium Bicarbonate
Na <sub>2</sub> SO <sub>4</sub>	-	Sodium Sulphate
RT	-	Room Temperature
TLC	-	Thin layer chromatography
NMR	-	Nuclear magnetic resonance

UV-Vis - Ultraviolet Visible

nm - Nanometer

$^1\text{H}$ -NMR - Proton NMR

$^{13}\text{C}$ -NMR - Carbon-13 NMR

# Abstract

Three acceptor-donor (AD) molecular rotor compounds were synthesized and characterized in this work whereby dyads **p-AD** and **m-AD** and triad **m-ADA** contained BODIPY and Benzodithiophene (BDT) as electron acceptor and donor respectively. In all the compounds, the donor and acceptor moieties are electronically decoupled by a phenyl spacer, either through a para coupling or through a Meta coupling. Through spectroscopic studies, structure property relationships have been deduced in this work. Earlier, **p-ADA** was synthesized based on BODIPY dye as acceptor and BDT as electron donor decoupled with a para-phenyl spacer. The compound showed dual emission with efficient twisted intramolecular charge transfer (TICT) band at  $\sim 700$  nm with Stokes shift of  $\sim 194$  nm. Prominent fluorescence solvatochromism in solvents of increasing polarity was observed for **p-ADA**. Efficient aggregate induced emission and a reasonable charge carrier mobility of **p-ADA** in thin films of  $\sim 4 \times 10^{-4}$  cm<sup>2</sup>/Vs. However, meta regioisomeric triad **m-ADA** showed well-defined aggregation in solution evident from absorption and emission studies. On the other hand, the dyad counterparts of these two compounds **p-AD** and **m-AD** showed distinct photophysical characteristics whereby the dyad **p-AD** showed multiple emissions with TICT band at 660 nm characterized by a smaller Stokes shift of  $\sim 149$  nm and prominent solvatochromism. Notably, all compounds showed temperature tunable and viscosity dependent emission changes. The temperature dependence of emission intensities of **p-AD** and **p-ADA** render these molecules useful ratiometric sensors. On the other hand, viscosity dependence of fluorescence is indicative of their potential applications as viscosity sensors for biologically or material science relevant micro-environments. This study substantiates the fact that by subtle and minimal variations in the chemical structures, optical and electronic properties of such rotor molecules can be tuned to a great extent that have potential applications in biolabelling and sensing. Such multifunctional rotor molecules with readily tunable emission properties are potential temperature and viscosity sensors for bio(medical) and material applications.

# Chapter 1

## Introduction

### 1.1 4,4-Difluoro-4-bora-3a,4a-diaza-s-indacene (BODIPY)

BODIPYs are a class of emerging dyes which are extensively used in organic photovoltaics (OPV) with several advantages such as strong absorption at higher wavelength, high quantum yield, high thermal and photo stability, tunable redox and fluorescence, high molar extinction coefficient etc. These kind of small organic molecules have advantage over polymer because of their ease of synthesis and batch-to-batch reproducibility of yields, purification and further characterization. BODIPYs have been extensively used for bioimaging and biolabeling.<sup>1,2</sup>

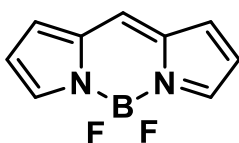


Fig. 1.1 BODIPY core

### 1.2 Benzodithiophene (BDT)

Benzodithiophene (BDT) are used in OPV application due to its planar structure which contributes  $\pi$ - $\pi$  stacking and thus efficient charge transport. The solubility and intermolecular interactions can be tuned by varying the substituents in BDT. Deep lying HOMO levels and high power conversion efficiency make BDT an important class of molecule in the design of organic semiconductors and organic semiconducting polymers.<sup>3</sup>

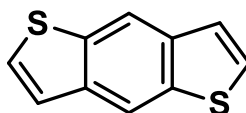
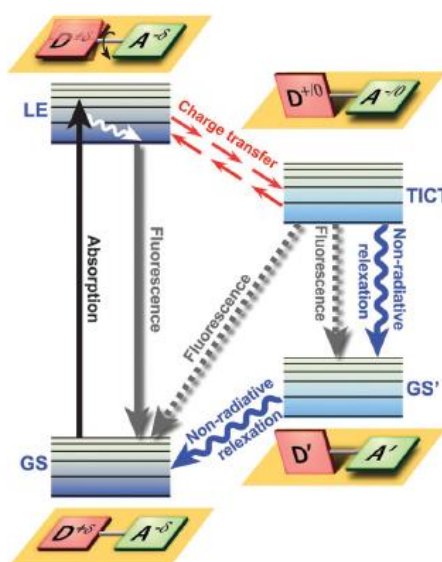


Fig. 1.2 BDT core

### 1.3 Twisted Intramolecular Charge Transfer state

TICT is an electron transfer process which is observed upon photoexcitation of a molecule containing a donor and acceptor linked by a single bond. Upon photoexcitation, there is a rotation of the bond connecting the donor and acceptor that leads to charge separation in excited state. Such a charge separated state has a very high dipole moment. After intramolecular twisting, the TICT state returns to ground which results in a red emission or a nonradiative relaxation. There will be also an emission from the planar excited state, the so-called local excited (LE) state and this results in dual emission i.e., two emissions from the LE state and the TICT state.



**Fig. 1.3** Twisted Intramolecular Charge Transfer Dynamics. (Courtesy : Recent advances in twisted intramolecular charge transfer (TICT) fluorescence and related phenomena in materials chemistry)<sup>4</sup>

While undergoing TICT, the molecule itself goes through several conformations. If the molecule contains a donor and acceptor separated by a single bond, the twisting will occur. In polar environment, fast electron transfer occurs from donor to acceptor which is accompanied by twisting in D-A single bond. The molecule is in planar conformation in the ground state, but in TICT state it will attain a perpendicular structure followed by a large change in the dipole moment. So in excited state, the molecule attains a coplanar structure in locally excited state and a relaxed perpendicular structure in TICT state. There is equilibrium between these two conformations which result in dual fluorescence,

one from a high energy band through relaxation from locally excited (LE) state and one from the lower energy band due to TICT. The emission from the TICT state results in high pseudo Stokes shift since the (HOMO-LUMO) energy gap is small.

The relaxation pathways can be modulated by changing the substituents and chemical modification of the structures, polarity of the medium, temperature and so on. Thus, TICT is an important photophysical process can be used to tune the fluorescence over a wide emission color range, hence it can be exploited in applications such as organic light emitting diodes (OLEDs), temperature sensors, viscosity sensors, bio-imaging, bio-labeling, nonlinear optics, chemosensors and organic photovoltaics.<sup>4,5</sup>

### **1.3.1 Solvatochromism**

Solvatochromism is the process by which the solute will show different colors in solvents of different polarities. It mainly depends on the dielectric constant of the solvent and H- bonding ability. The most important parameter that leads to solvatochromism is the molecular structure itself, which should have sites for charge separation that can give rise to a permanent dipole moment. A donor-acceptor type molecule is a good example where, positive and negative charges can localize on the donor and acceptor respectively and give rise to a high dipole moment (in ground state or upon photoexcitation). If the ground state of the molecule has a high dipole moment than the excited state, it is more stabilized in polar solvents, thus upon increasing polarity of the solvent, the absorption peaks shift hypsochromically which is known as negative solvatochromism. On the other hand, when the excited state has a higher dipole moment than the ground state, it is more stabilized in polar solvents, then on increasing polarity of solvent it will show a bathochromic shift, this is termed positive solvatochromism. By changing solvent polarities, it is possible to tune the HOMO-LUMO energy gaps. Thus in solvents of different polarities, pronounced changes in the absorption or emission spectra such as changes in peak positions, intensities or even the shape of the spectra can be observed.

In case of TICT state, since the excited state has a higher dipole moment due to twisting and charge separation, it will get preferentially stabilized in the polar solvents compared to non-polar solvents. Moreover, TICT is an excited state thus, upon increasing the polarity of the solvent, a bathochromic shift in the emission spectra is observed for the TICT band.



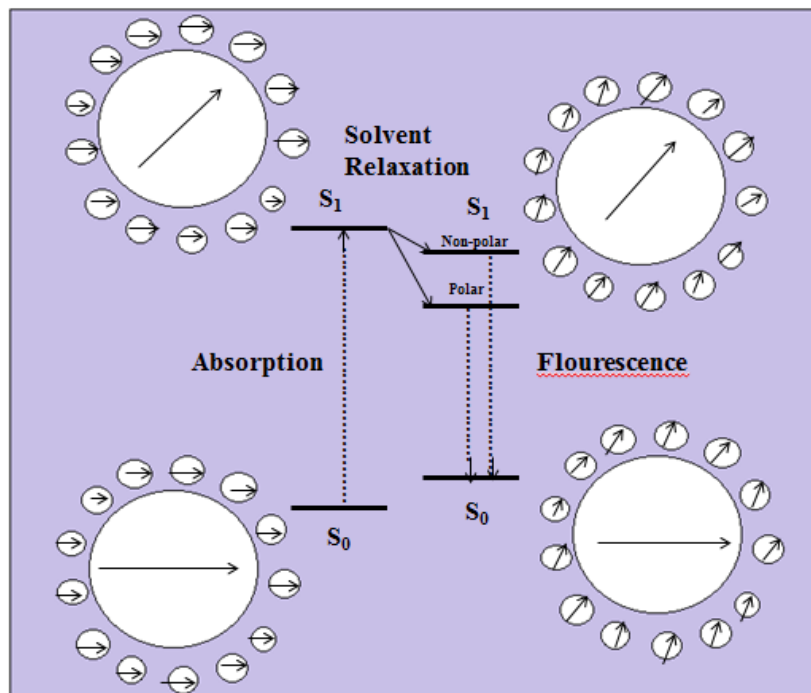


**Fig. 1.4** Solvent effects on electronic state energies.  $S_0$  is the ground state,  $S_1$  is the excited state, dashed line: radiative process, solid lines: non-radiative processes. (Adapted from Cecil and Rutan.)

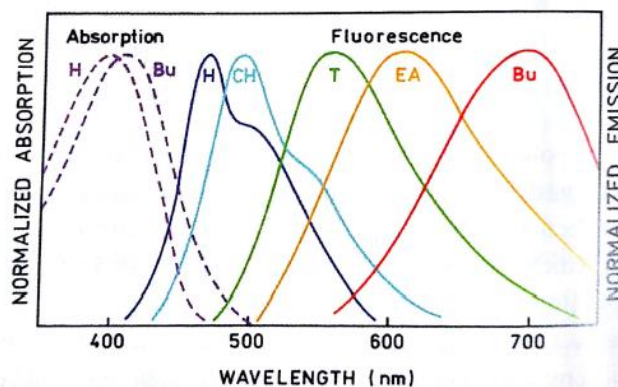
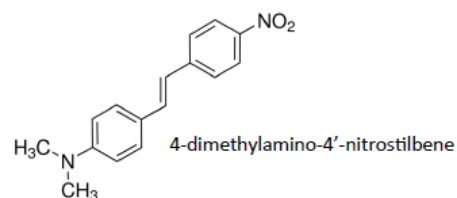


**Fig. 1.5** Solvatochromism observed in 4-dimethylamino-4'-nitrostilbene on increasing the solvent polarity from hexane to butanol (courtesy : Principles of Fluorescence Spectroscopy, J. Lakowicz)

## 1.4 Aggregate Induced Emission

Aggregate induced emission is an unusual photophysical phenomenon shown by molecules when molecularly dissolved species are introduced in a bad solvent leading to their aggregation and due to restricted rotation, an enhancement in the emission intensity. Upon increasing the percentage of water, the molecular rotors will form a well-defined nano aggregates that restricts the intramolecular rotations causing the equilibrium to shift towards LE state leading to increase in the fluorescence intensity. Non polar solvent are highly hydrophobic so rotor type molecules adopt a planar conformation and show only local excited (LE) state emission. In polar solvents which have high hydrophilicity, conformation of molecule is twisted and leads to the formation of TICT state, which red-shifts and weakens the emission of the fluorophore. When water is added into THF, the molecules cluster to form nanoaggregates due to restricted intramolecular rotations. This leads to enhancement in emission intensity compared to the TICT state emission.

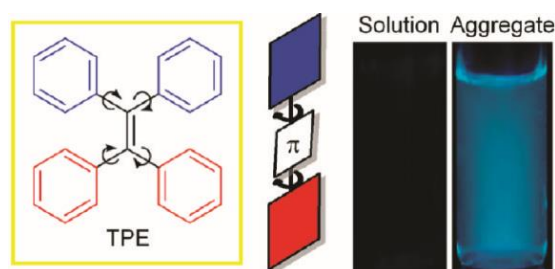


**Fig. 1.6** Aggregation-induced emission (AIE). Intramolecular rotation makes tetraphenylethene (TPE) non-luminescent in the solution state, whereas restriction of the intramolecular rotation makes it highly emissive in the aggregate state, in dilute solution of TPE in acetonitrile and for its aggregates suspended in an acetonitrile/water mixture with 99% water under UV illumination. (Courtesy : *J. Phys. Chem. C*, Vol. 113, No. 36, 2009).

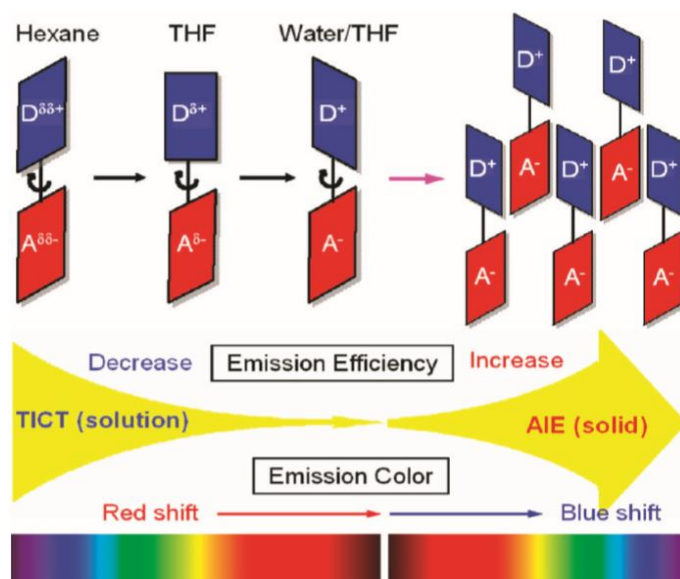


**Fig. 1.7** Proposed Mechanism for TICT and AIE Processes in BODIPY Luminogens (Courtesy : *J. Phys. Chem. C*, Vol. 113, No. 36, 2009).

### 1.5 Temperature Sensing

Molecular rotors are highly sensitive to temperature and show different emission properties on varying the medium temperature. Temperature sensing in rotor type molecules arises due to mostly two decay channels originating from two molecular conformations (i.e., TICT and planar or LE states) at the excited state. At higher temperatures, faster molecular rotations lead to non-radiative decay and thus decrease in fluorescence intensity. In some cases increasing temperature leads to increase in emission intensity because high temperature provides the activation energy that assists the excited electron in crossing the activation barrier from TICT to the LE state and LE state gets more populated.<sup>6,5</sup>

### 1.6 Viscosity Sensing

TICT type rotor based fluorophores are sensitive to viscosity and their viscosity sensing can be used for quantitative measurements of microscopic viscosity. For better results, we should use a small molecular sensor with cell permeability. At the cellular level, many diseases are characterized by a change of viscosity of the intracellular fluids of the diseased cells. The existing methods for measuring viscosity such as falling ball viscometer, capillary viscometer etc.<sup>7</sup> cannot be applied at cellular level. Molecular rotors being sensitive to viscosity are thus well suited for viscosity

measurements and can be used for measurement of microviscosity. Due to the presence of rotatable bonds, their fluorescence is quenched in non-viscous solution, it will result in a weak intrinsic fluorescence.<sup>7,8</sup> If the rotation of the bonds are restricted by using a viscous media then the fluorescence emission will increase.

Some examples were reported in literature where the intramolecular rotations were restricted and microviscosity was measured. In Suhling et. al.<sup>9</sup> they have reported a dipyrin related fluorescent sensor in which rotation of the phenyl group is restricted and thus by imaging microviscosity was measured. A RY3 fluorescent sensor was reported where the aldehyde group act as rotor to measure intracellular viscosity.<sup>10</sup> Luby-Phelps reported a ratiometric system of fluorescent Cy5 and Cy3 which was attached to Ficoll 70 to measure microviscosity.<sup>11</sup> Thus by monitoring the viscosity of biofluid it will provide a diagnostic tool for detection of diseases.

The basics of the ratiometric sensing is that on increasing viscosity the red emission is greatly enhanced while the blue emission remains intact.

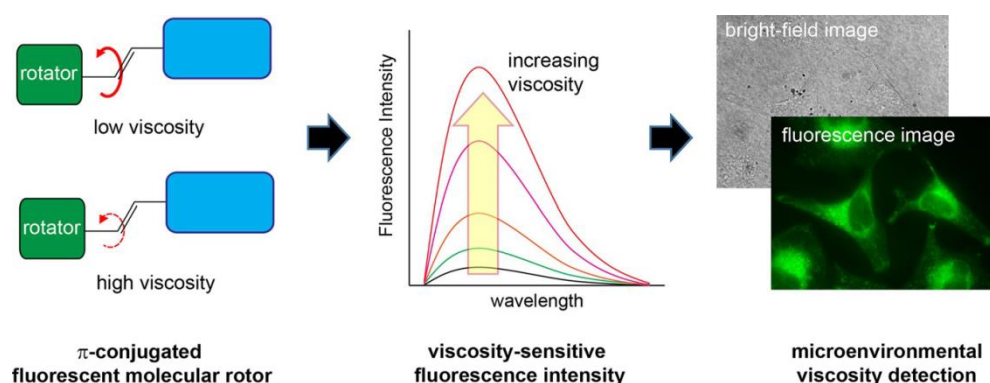


**Fig. 1.8** General chemical structure of fluorescent molecular rotors (FMRs) with its working principle. (Courtesy : *Chem. Eur. J.* 10.1002/chem.201801389).

For BODIPY dyes which show TICT emission and AIE have found to show high Stokes shift. But one of the disadvantages is that if the number of rotatable junctions in a molecule are increased, the fluorescence quantum yield decreases. Although BODIPYs are well-known molecular rotors, only few examples are known in the literature where TICT and AIE have been employed in the same molecules.<sup>12,13,14</sup> Recently one work was published on a molecular rotor namely, acceptor–donor–acceptor (A–D–A) triad based on a BODIPY acceptor and a benzodithiophene donor which are electronically decoupled by a para phenyl spacer.<sup>13</sup> This molecule exhibited dual fluorescence and pronounced fluorescence solvatochromism because of twisted intramolecular charge transfer (TICT)

state formation. This compound showed a pseudo Stoke shift of ~194 nm which is highest known for any BODIPY compound.

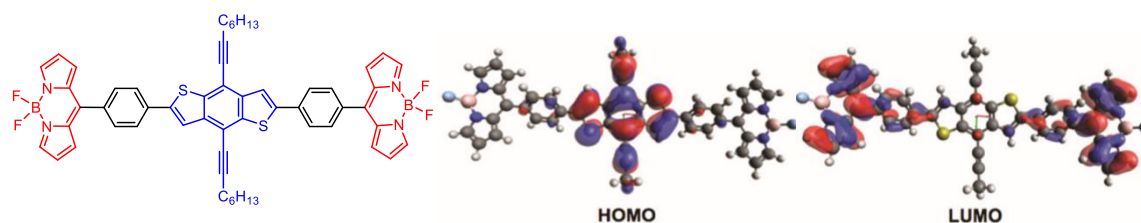


**Fig. 1.9** (a) Molecular structure of **p-ADA** in which BODIPY and BDT is separated by phenyl spacer. (b) HOMO-LUMO of **p-ADA** by DFT calculations using B3LYP/6-31G (d,p).

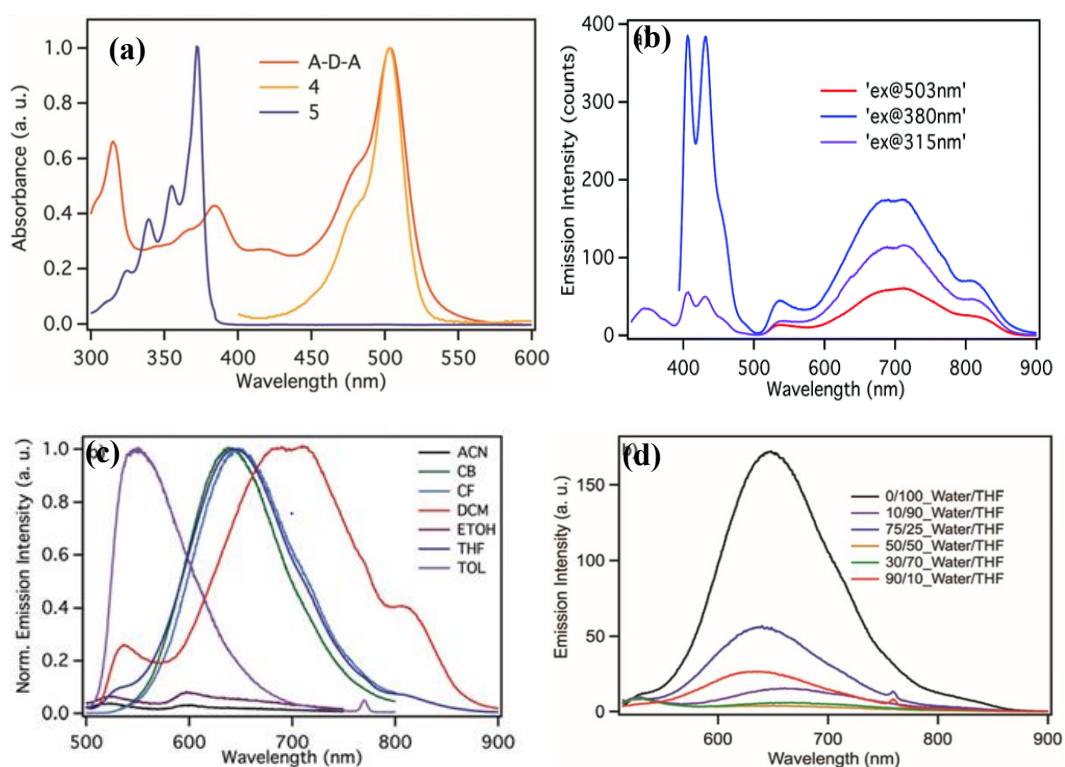


**Fig. 1.10** (a) UV-Vis absorption spectra of model compounds 5, 4 and triad **A-D-A** in DCM. (b) Fluorescence emission spectra of **p-ADA** in DCM. (c) fluorescence emission spectra of **A-D-A** upon excitation at 380 nm in acetonitrile (ACN), chlorobenzene (CB), chloroform (CF), ethanol (EtOH), toluene (Tol) and DCM and (d) AIE formation in **A-D-A** in various weight fractions of water and THF.<sup>13</sup>

The HOMO-LUMO energy gaps were calculated by density functional theory (DFT) calculations and for **p-ADA**, the HOMO is entirely localized on the BDT unit and the LUMO entirely localized on BODIPY with no overlap between the HOMO and LUMO (Fig. 1.9 b). Hence there is no electronic communication between BODIPY and BDT. This observation was further confirmed by electronic absorption spectrum (Fig. 1.10 a). For individual monomer the absorption maxima of donor was found to be at 372 nm and absorption maxima of acceptor at 504 nm respectively. For **p-ADA** the absorption spectrum was merely the sum of individual monomer spectrum.

From fluorescence emission spectra the molecule was found to be dual emissive (Fig. 1.10 b). Other than a donor emission around ~ 405 nm, a broad but intense emission was observed around ~ 698 nm. This was attributed to twisted intramolecular charge transfer. A pseudo Stokes shift of ~ 194 nm was obtained which is highest known for any BODIPY compound. Calculation of torsional angles as well as the dipole moment of ground state and the excited state justified the formation of TICT state.

A positive solvatochromism was observed for **p-ADA** due to stabilization of TICT state in polar solvents (Fig. 1.10 c). On increasing the polarity of the solvent from toluene to DCM, a transition of LE state to TICT state was observed. A pronounced AIE was also exhibited by this molecule (Fig. 1.10 d). On increasing the fraction percentage of water solvent polarity twisted the molecule and equilibrium shifted towards TICT state which resulted in a bathochromic shift. Upon increasing to 75% and 90% fraction percentage of water, the **p-ADA** preferably forms well-defined Nano aggregates which lead to restricted intramolecular rotation (RIR) which causes the equilibrium towards LE state and LE state gets more populated, thus results in increased fluorescence intensity.

A high hole mobility of  $4.45 \times 10^{-4} \text{ cm}^2 \text{ V}^{-1} \text{ s}^{-1}$  was obtained for **p-ADA** so that it is suitable for (opto) electronic applications such as in OLEDs and in OPVs. It is suitable for OLED applications since AIE was observed for **p-ADA** in solvent mixtures of hexane/water with emission intensity and wavelength varying with increasing fraction percentage of water.

## 1.7 Our objective

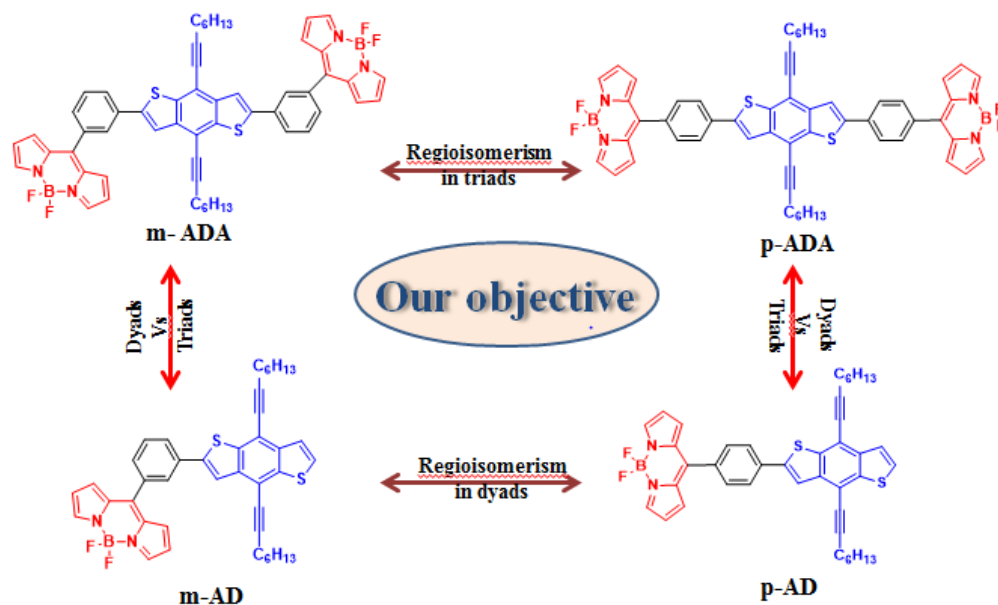


**Fig. 1.11** Molecular Design principle of our work

Our objective in this work is to synthesize some rotor molecules based on our recently published design principle, a meta substituted acceptor-donor-acceptor **ADA** triad (**m-ADA**) and corresponding acceptor-donor dyad compounds **AD** dyads (**p-AD** and **m-AD**) with BODIPY as acceptor and BDT as donor electronically separated by a phenyl spacer either through para coupling (**p-AD**, **p-ADA**) or through meta coupling (**m-AD**, **m-ADA**) to study TICT, dual fluorescence, solvatochromism, AIE and other related properties. Regioisomerism in triads and dyads were compared and the effects of TICT in dyad compounds were also investigated. Instead of 4 rotatable bonds like in case of **p-ADA**, there are only two rotatable junctions in case of **p-AD** so we expected to see less TICT effect compared to its triads. So the dyads and triads have been also compared in this work.

As discussed earlier, rotor type molecules are extremely sensitive to solvent polarity effects, temperature and viscosity of the medium. Due to their environment sensitivity, these molecules can be exploited in different applications. The fluorescence emission intensity can be tuned by varying temperature and viscosity. These kind of molecular rotors are well suited for temperature and viscosity sensing for biologically relevant systems or in materials science. We expected some of the designed compounds to show

TICT which will decrease the fluorescence emission intensity thus decreasing fluorescence quantum yield. In this work, we have performed a systematic study of all the TICT, solvent dependent emission, temperature and viscosity effect on emission intensities of all compounds.

In this work, we deduce structure property relationships of the designed and synthesized molecules and it will be shown that even though the structures are closely related i.e., regioisomers (**p-ADA** vs **m-ADA**; **p-AD** vs **m-AD**), their optical and photophysical properties are distinct and completely different from each other. This study substantiates the fact that by subtle and minimal variations in the structures, optical and electronic properties of such rotor molecules can be tuned to a great extent that have many potential applications in bio labeling and sensing.

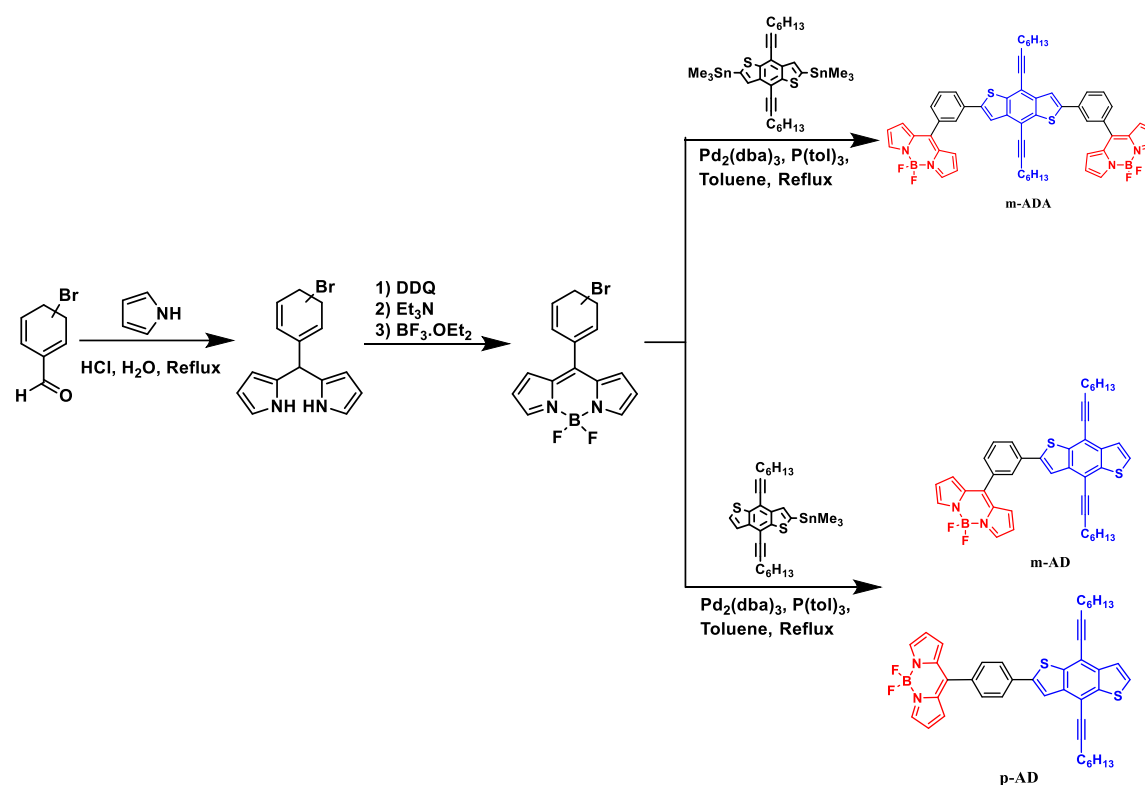
Such multifunctional rotor molecules with readily tunable emission properties are potential temperature and viscosity sensors for bio (medical) and material applications.



# Chapter 2

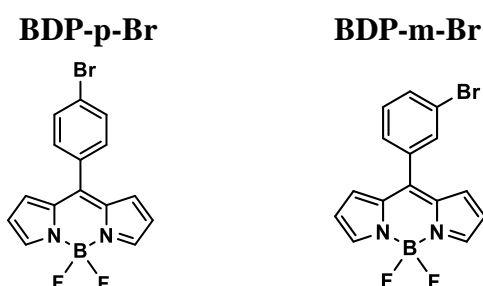
## Results and Discussion

We commenced our project following Scheme 2.1 Synthesis of BODIPY was carried out using DDQ as oxidant which was followed by boron insertion with  $\text{BF}_3 \cdot \text{OEt}_2$ . Further Stille coupling between di or mono substituted BDT with BODIPY was carried out with palladium and Tris(o-tolyl)phosphine catalyst.



**Scheme 2.1** General synthesis scheme for synthesis of m-ADA, m-AD and p-AD

The two regioisomeric BODIPY acceptor compounds were characterized using UV-VIS absorption and fluorescence spectroscopy in both solution and in thin films. Figure 2.1 compares the optical properties of **BDP-p-Br** and **BDP-m-Br** in solution and thin film.



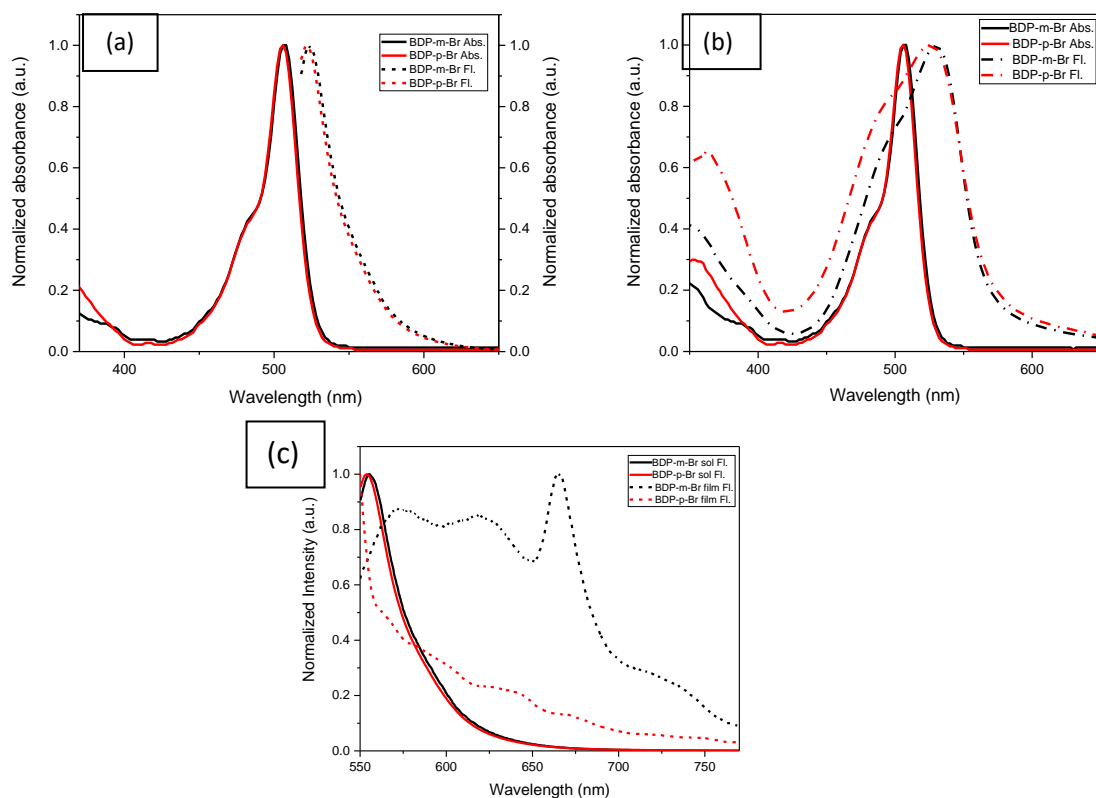


**Fig. 2.1** Optical properties of **BDP-p-Br** and **BDP-m-Br** in chloroform for  $c \sim 10^{-5}M$  : (a) Normalized absorption and emission spectra of **BDP-p-Br** and **BDP-m-Br** in solution. (b) Normalized absorbance of **BDP-p-Br** and **BDP-m-Br** in solution Vs. thin films spin-coated (from 5 mg/mL solution) on quartz substrates at 500 rpm. (c) Normalized emission spectra of **BDP-p-Br** ( $\lambda_{exc}$  506 nm for solution and 526 nm for film) and **BDP-m-Br** ( $\lambda_{exc}$  508 nm for solution and 530 nm for film).

Fig 2.1a represents the normalized absorbance and fluorescence of both the regioisomeric BODIPYs. The absorption maxima of BODIPYs were found to be 506 nm and 508 nm for **BDP-p-Br** and **BDP-m-Br** respectively. The **BDP-m-Br** was red shifted than the **BDP-p-Br** by 2 nm. From analyzing the  $\epsilon$  value of two BODIPYs obtained by calibration curves of absorbance recorded at 5 different concentrations, **BDP-m-Br** showed an  $\epsilon$  of  $55400 M^{-1}cm^{-1}$  and **BDP-p-Br** showed an  $\epsilon$  of  $42000 M^{-1}cm^{-1}$ . Thus, **BDP-m-Br** has higher molar absorptivity than **BDP-p-Br**.

Thin films of these compounds were prepared by spin coating solutions of these compounds (in  $CHCl_3$ , 5 mg/mL) onto quartz substrates at 500 rpm. Absorption of these thin film samples were recorded and for **BDP-m-Br** (Fig 2.1b), the absorption maxima

was observed at 530 nm while in solution it was observed at 508 nm, i.e., it was red shifted by 22 nm. On the other hand, for **BDP-p-Br** it was red shifted by 20 nm.

The normalized fluorescence of thin films shows distinct differences from solution fluorescence (Fig 2.1c). In thin films, the emission spectra broadened significantly and were bathochromically shifted for both BODIPYs. Compared to **BDP-p-Br**, the meta counterpart showed more broadening and showed a prominent peak around ~ 666 nm. Both BODIPYs showed three peaks (Table 1), however, in each case the peak positions were red shifted in **BDP-p-Br** compared to **BDP-m-Br** compound.

**Table 1** : Comparison of  $\lambda_{ab}^{max}$  and  $\lambda_{em}^{max}$  of **BDP-m-Br** and **BDP-p-Br** in solution and thin films in chloroform at  $c \sim 10^{-5}$  M.

Compounds	Solution			Thin Film	
	$\lambda_{ab}^{max}$ (nm)	$\lambda_{em}^{max}$ (nm)	$\epsilon$ ( $M^{-1}cm^{-1}$ )	$\lambda_{ab}^{max}$ (nm)	$\lambda_{em}^{max}$ (nm)
<b>BDP-m-Br</b>	508	523	55400	530	574, 620, 666
<b>BDP-p-Br</b>	506	521	42000	526	589, 635, 670

### Density Functional Theory (DFT) Calculations

In order to gain insights about the frontier molecular orbitals (FMOs) of the synthesized molecules as well as the geometrical parameters of the structures (bond angles, torsion angles), density functional theory (DFT) calculations were performed for all molecules. The highest occupied molecular orbital (HOMO) and lowest unoccupied molecular orbital (LUMO) levels of **m-ADA**, **m-AD** and **p-AD** were calculated by the density functional theory (DFT) calculations using the Gaussian 09 package by the B3LYP/6-31G(d,p) method. For **m-ADA**, HOMO was entirely localized on BDT unit and LUMO partially localized on BODIPY and phenyl unit with no overlap between the HOMO and LUMO (Fig.2.2).

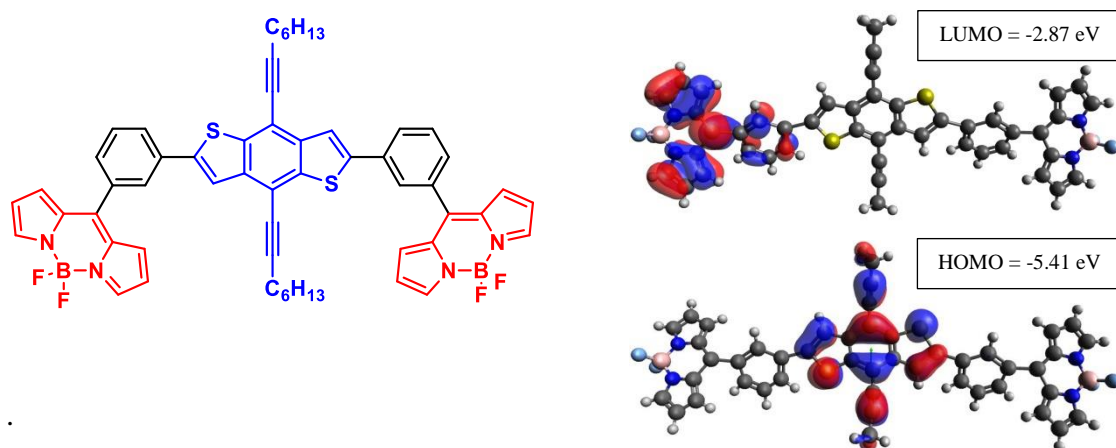


**Fig. 2.2** Orbital plots of HOMO and LUMO of **m-ADA** calculated by B3LYP/6-31G(d,p) method, plots have isodensity surface of 0.02.

Therefore, no electronic communication was present between BDT and BODIPY and this observation was confirmed later by experimental absorption spectrum of **m-ADA**. Upon performing geometry optimization on **m-ADA**, the torsional angles between the BODIPY and phenyl spacer ( $\Phi_1$ ,  $\Phi_4$ ) and between phenyl spacer and BDT ( $\Phi_2$ ,  $\Phi_3$ ) were found to be  $\sim 55^\circ$ ,  $54.2^\circ$  and  $\sim 22^\circ$ ,  $25.3^\circ$  respectively (Table 2). Such torsion angles confirm the non-planarity of this molecule. Moreover, the calculated HOMO and LUMO energy levels of **m-ADA** were found to be -5.41 eV and -2.87 eV respectively.

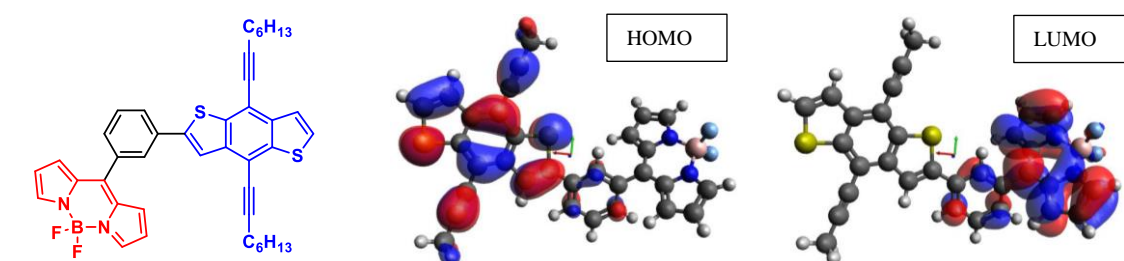


**Fig. 2.3** Orbital plots of HOMO-LUMO of **m-AD** by B3LYP/6-31G(d,p) geometry optimization method.

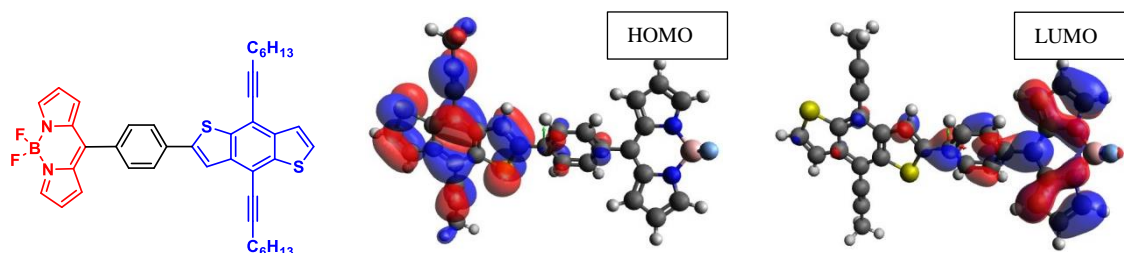


**Fig. 2.4** Orbital plots of HOMO-LUMO of **p-AD** by B3LYP/6-31G(d,p) geometry optimization method.

Similar results were obtained from DFT calculations on the dyad compounds p-AD and m-AD. HOMO and LUMO of both **m-AD** and **p-AD** were entirely localized on BDT and BODIPY respectively (Fig 2.3 & Fig 2.4). Hence there was no electronic communication between BDT and BODIPY units, same as in **m-ADA** discussed above or p-ADA case.<sup>13</sup> The FMO distribution plots of all compounds indicate that donor and acceptor are electronically decoupled. However, coupling of phenyl ring with BDT is present in all cases and this coupling is very different in **m-ADA** when compared to p-ADA or in case of dyads **m-AD** and **p-AD**. The result of these distinct coupling are reflected in their optical properties which have been discussed later.

The HOMO and LUMO energy levels of **m-AD** are at -5.30 eV and -2.79 eV while the HOMO and LUMO levels of **p-AD** are at -5.33 eV and -2.79 eV respectively. Thus, upon comparing the two dyads, **p-AD** has a slightly more stabilized HOMO level (-5.33 eV) compared to the **m-AD**. Torsion angles between the BODIPY and phenyl spacer ( $\Phi_1$ ) and between phenyl spacer and BDT ( $\Phi_2$ ) in m-AD were 54° and 23.9° respectively while in **p-AD** they were 55° and 22° respectively (Table 2). Hence the non-planarity of these dyad molecules is confirmed. All the torsion angles of the newly synthesized dyads and triad compare well with our previously reported **p-ADA** compound<sup>13</sup> and these results have been compiled in table 2.

**Table 2 :** Torsion angles (degree) and HOMO LUMO (eV) energy level calculated by B3LYP/6-31G (d,p) of dyads and triads.

Compound	$\phi_1$ (deg)	$\phi_2$ (deg)	$\phi_3$ (deg)	$\phi_4$ (deg)	HOMO (eV)	LUMO (eV)
<b>m-ADA</b>	55	22	25.3	54.2	-5.41	-2.87
<b>m-AD</b>	54	23.9	-	-	-5.30	-2.79
<b>p-AD</b>	55	22	-	-	-5.33	-2.79
<b>p-ADA</b>	54.1	32.2	32.2	55.8	-5.86	-3.89

## Electronic absorption

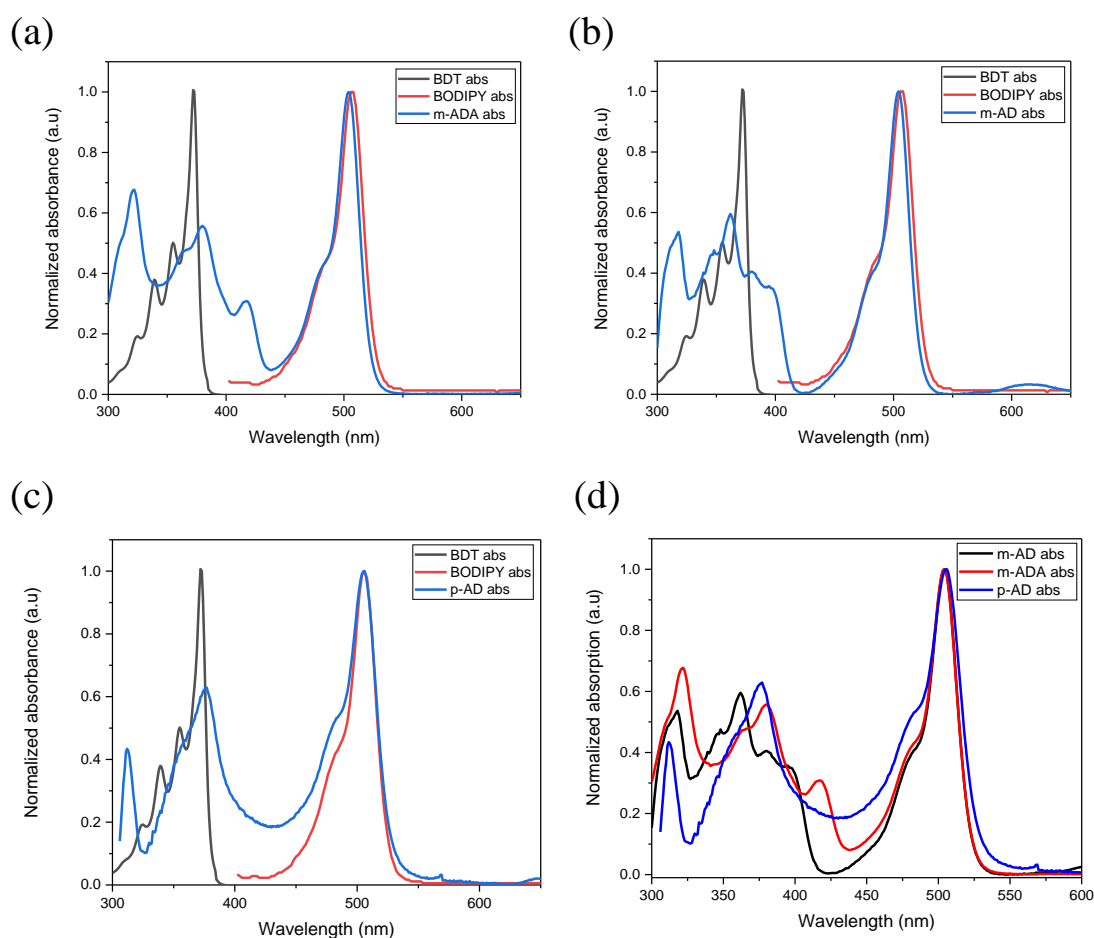


**Fig. 2.5** Normalized absorption spectra of (a) **m-ADA**, (b) **m-AD** and (c) **p-AD** compared with absorption of the acceptor BODIPYs and donor BDT in chloroform ( $c \sim 10^{-5}$  M). (d) Comparison of absorption spectra for **m-AD**, **p-AD**, **m-ADA** in chloroform ( $c \sim 10^{-5}$  M).

The absorption spectrum of m-ADA, m-AD and p-AD was compared with their corresponding monomer units, i.e., donor and acceptor units. All three compounds have three major peaks corresponding to BODIPY ( $\sim 505$  nm), BDT ( $\sim 312$ - $322$  nm), and broad peak around  $\sim 360$ - $380$  nm corresponding to extended conjugation of phenyl unit with BDT (Fig. 2.5). Peaks around  $\sim 505$  nm correspond to BODIPY  $S_0$ - $S_1$  transition and  $312$ - $322$  nm to BDT  $\pi$ - $\pi^*$  transition. Notably, no electronic communication was observed between BDT and BODIPY since the individual peak positions of BDT and BODIPY are maintained in the dyads and triad compound. This observation is in agreement with the DFT calculations showing compartmentalization of HOMO and LUMO on the donor and acceptor respectively. Owing to the weaker coupling of m-phenyl with the BDT unit

compared to stronger coupling in p-phenyl with BDT, peak splitting was observed more in meta compounds (Figures 2.5a and 2.5b) than compared to the Para compound (Fig. 2.5c)

**p-AD** (Fig. 2.5d) shows the comparative absorption spectra of all the three compounds i.e., dyads **p-AD**, **m-AD** and triad **m-ADA**.

### Steady-state fluorescence

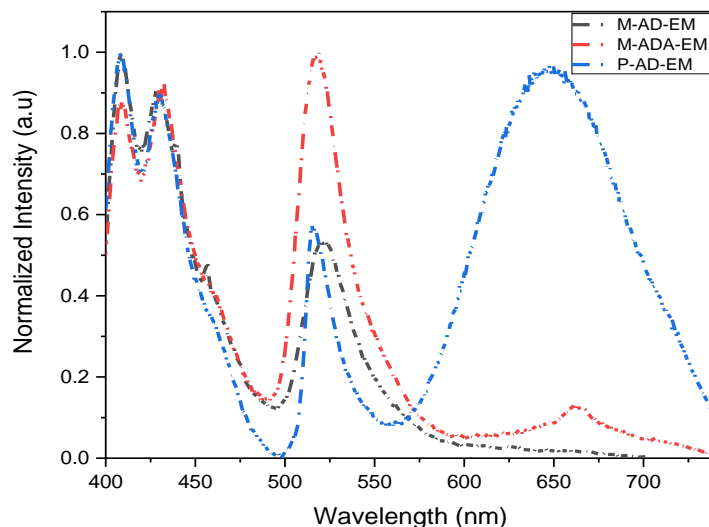


**Fig. 2.6** Normalized emission spectra for **m-AD**, **p-AD**, **m-ADA** in Chloroform ( $c \sim 10^{-5}$  M) upon exciting at 362 nm, 377 nm, and 380 nm respectively.

Fluorescence emission spectra of **m-ADA** were measured upon three different wavelengths, 322 nm, 380 nm (donor) and 504 nm (acceptor) respectively. Upon excitation at 322 nm and 380 nm, donor emission at 430 nm, acceptor emission at 517 nm and a broad but less intense band around  $\sim 662$  nm were observed. The band around  $\sim 662$  nm was found to be due to aggregation which was confirmed by absorption spectroscopy (Fig. 2.6). Triad **m-ADA** was found to be a multiple emissive chromophore and formed aggregates in such a very low concentration.

In case of **m-AD**, three distinct emission peaks were observed. Upon excitation at 362 nm (donor) and 504 nm (acceptor), a donor emission peak at 430 nm and acceptor emission at 522 nm were observed. A broad but a weaker TICT band was formed around  $\sim 645$  nm. This was further confirmed by performing fluorescence solvatochromism study in hexane/THF mixture.

The fluorescence emission spectra of **p-AD** were measured upon excitation at two wavelengths 377 nm (donor) and 506 nm (acceptor). Excitation at 377 nm led to emission at 430 nm from donor, 516 nm from acceptor and a broad but intense band around ~ 654 nm corresponding to a twisted intramolecular charge transfer state (TICT). A pseudo-Stokes shift of ~149 nm was observed which was expected upon comparing with **p-ADA**. Such Stokes shift is unusually high for these classes of compounds. The corresponding **p-ADA** was found to have a remarkable Stokes shift of 194 nm, highest known Stokes shift till date for any BODIPY compound.<sup>13</sup> The formation of the TICT state in **p-AD** can be attributed to the high torsional angles (DFT calculated) as well as possibility of stronger charge separation between the donor and acceptor in the excited state similar to the earlier reported **p-ADA** compound. However, owing to the lesser number of rotatable junction in **p-AD** (two) Vs. the **p-ADA** (four) compound, Stokes shift was about 45 nm less in case of p-AD (149 nm) compared to **p-ADA** (~194 nm).

**Table 3:** Absorption and Emission of dyads and triads in chloroform ( $c \sim 10^{-5}$  M)

Compounds	m-ADA	m-AD	p-AD
Absorption (nm)	320, 380, 504	362, 504	312, 377, 506
Emission (nm)	430, 517, 662	430, 522, 645	430, 516, 654

### Fluorescence Solvatochromism

Solvatochromism is the process in which the color shown by donor-acceptor chromophore is different in solvents of different polarity owing to the tuning of the optical gaps in solvents of different polarity. Solvatochromism mainly depends on permanent dipole moment of the molecule in the ground state and in excited state. If the molecule has a stronger dipole moment (and thus better charge separation) in the ground state that the excited state, the ground state gets preferentially more stabilized in polar solvents. As a result, the optical gap increases and the absorption or fluorescence are shifted hypsochromically. On the other hand, if the dipole moment of the excited state is higher than the ground state, it is stabilized in polar solvents more than the ground state leading to reduction in the optical gap and thus bathochromic shift in the emission.



Thus, upon increasing the solvent polarity, if the emission is blue shifted (hypsochromic shift) then molecule shows negative solvatochromism. A stabilized excited state on the other hand shows bathochromic shift upon increasing solvent polarity.

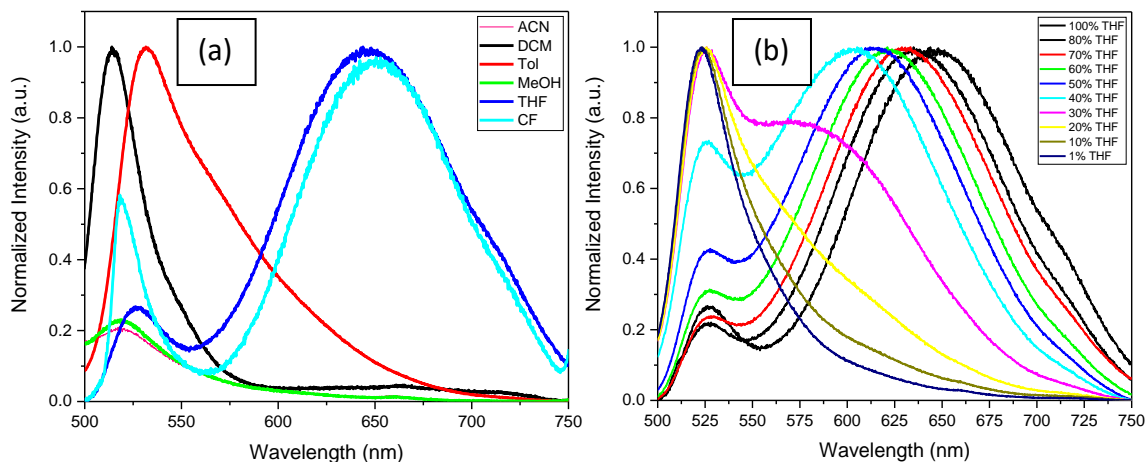


**Fig. 2.7** Normalized fluorescence emission spectra of (a) **p-AD** upon excitation at 377 nm in solvents of different polarity (b) in different hexane/THF (v/v) solvent mixtures.

Formation of TICT state in **p-AD** was justified from torsion angles calculated by DFT which results in twisting around the BODIPY-phenyl single bond and thus separating the D-A units in the excited state leading to pronounced charge separation of the donor and acceptor units and thus an increase in the dipole moment of the molecule in the excited state. Such increased dipole moment in the excited state is expected to show positive fluorescence solvatochromism which is indeed the case of **p-AD**. Due to such dissimilar dipole moments in excited and ground state, a pronounced positive solvatochromism is observed for **p-AD** on increasing the solvent polarity (Fig. 2.7a). Emission maximum from  $\sim 530$  nm in toluene was shifted to  $\sim 654$  nm in chloroform, resulting in a bathochromic shift of 124 nm. The ground state of the **p-AD** less polar than the excited state, because UV-VIS absorption spectra of molecule in solvents of different polarities did not show any change in the absorption maxima. Notably, the TICT band was non-existent in high polarity solvents such as DCM, ACN and MeOH owing to the limited solubility in ACN and MeOH as well as very rapid non-radiative decay leading to negligible emission intensity at 650 nm. These observations are consistent with similar TICT compounds that show negligible emission in ACN and MeOH.<sup>6</sup>

The fluorescence solvatochromism was further probed in solvent mixtures of hexane and THF because a better control of the solvent polarity i.e., sequential decrease of the solvent

polarity was achievable by varying the percentage of hexane and THF. An emission maximum of  $\sim 647$  nm in THF shifted to  $\sim 515$  nm in 100% THF to 99/1 (v/v) hexane/THF respectively. Interestingly, when the solvent polarity was decreased from 100 % THF sequentially up to 99/1 (v/v) hexane/THF, a complete transition of TICT to LE state (through a broad band at  $\sim 580$  nm corresponding to intermittent LE state) could be observed (Fig. 2.7b). The molecule thus showed pronounced hypsochromic shift on decreasing solvent polarity and this study further substantiates the formation of TICT in the **p-AD** compound.

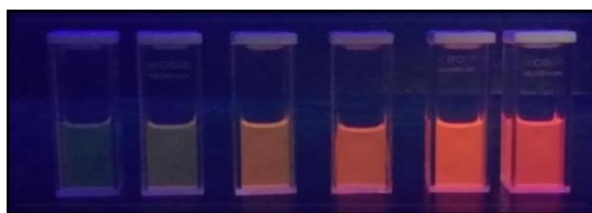


**Fig. 2.8** Fluorescence solvatochromism of **p-AD** in hexane/THF mixtures (from left to right: 99/1, 90/10, 80/20, 70/30, 60/40, 50/50 v/v hexane/THF) under UV lamp of wavelength 365 nm.

Interestingly, the meta counterpart **m-ADA** of our previous published compound<sup>13</sup> does not show any TICT even though it has four more rotatable junctions between donor and acceptor parts. Solvent polarity dependent fluorescence spectra of **m-ADA** showed a completely different behavior whereby apart from the BDT emission and BODIPY emission at 430 nm and 530 nm, a weak peak at  $\sim 660$  nm was observed in THF, toluene and a peak at  $\sim 675$  nm in MeOH and DCM was observed (Fig. 2.9a). The fact that this red-shifted peak is almost at the same position in polar and non-polar solvents indicate that this peak is not resulting due to TICT but due to formation of aggregates. The absence of any TICT in **m-ADA** could be attributed to the weaker electronic coupling between the donor and the acceptor through the meta positions of the phenyl. Moreover, triad **m-ADA** has no propensity for TICT could also be due to probably a higher activation barrier for twisted and planar states. Instead of TICT, **m-ADA** compound shows aggregation at such low concentrations of optical measurements ( $c \sim 10^{-5}$  M). A possible explanation for aggregation in **m-ADA** could be the comparable terminal ( $\phi_1$  and  $\phi_4$ ) twist angles of  $54^\circ$  and  $54.2^\circ$  to **p-ADA** and smaller middle twist angles ( $\phi_2$  and  $\phi_3$ ) of  $22^\circ$ ,  $25.3^\circ$  for **m-ADA** than **p-ADA** ( $32.2^\circ$ ,  $32.2^\circ$ ). Thus, **m-ADA** is actually less twisted than **p-ADA** and presumably has higher propensity to form intermolecular  $\pi$ -stacks and

thus aggregates. The aggregation of this compound is justified by a solvent dependent UV/Vis and fluorescence study of **m-ADA** in THF/hexane mixtures discussed in a later section, where increasing percentage of hexane clearly showed a color change from orange to pink and a red shifted band in the absorption spectra.

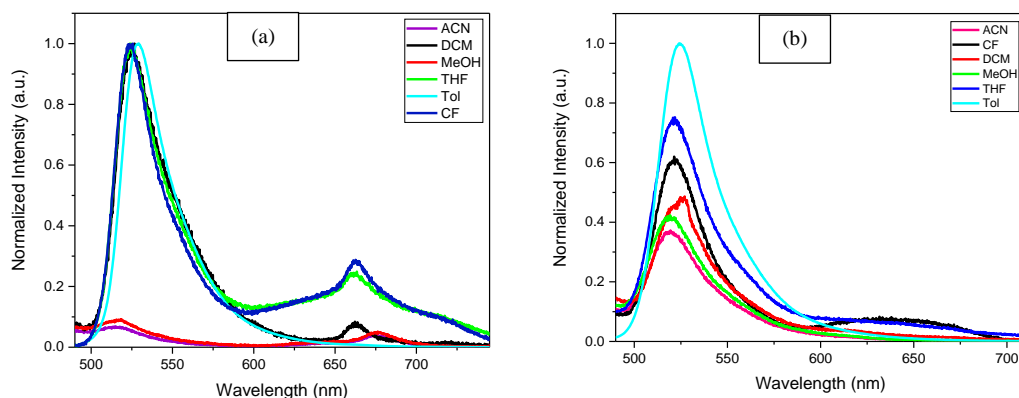


**Fig. 2.9** Fluorescence emission spectra of (a) **m-ADA** and (b) **m-AD** upon excitation at 380 nm and 362 nm respectively in different solvents.

Similar kind of solvatochromism studies were performed for **m-AD**. A weaker but a broad band around 643 nm was observed only in chloroform and THF which could be attributed to a very weak TICT-type transition (Fig. 2.9b).

### Aggregation induced emission (AIE)

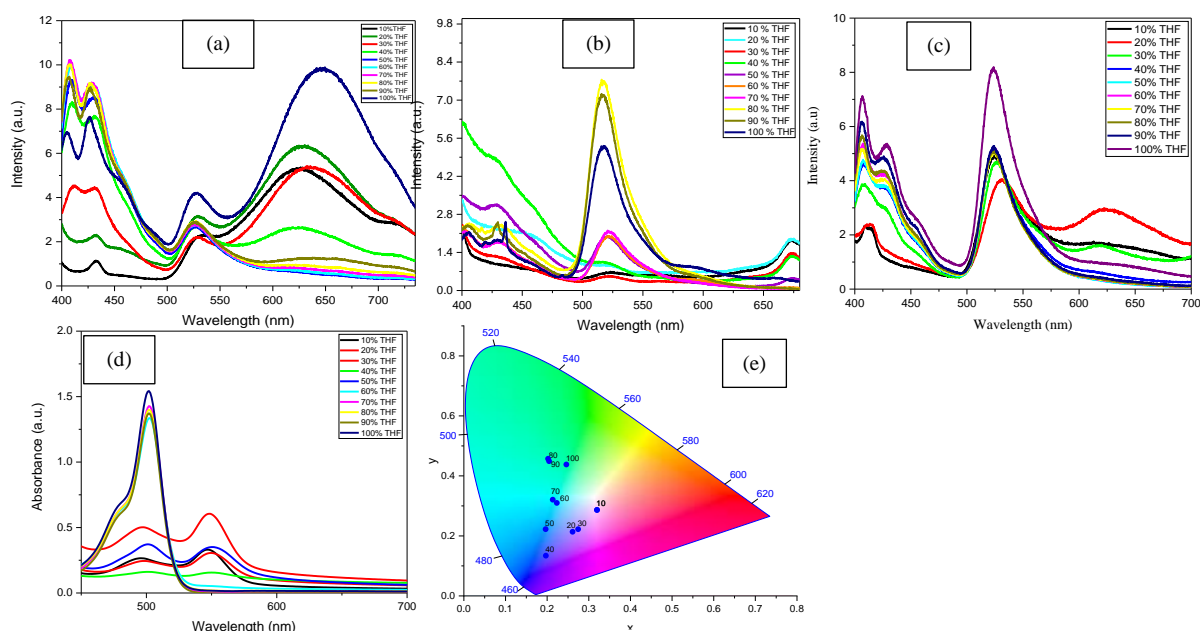


**Fig. 2.10** Aggregate induced emission in (a) **p-AD**, (b) **m-ADA**, and (c) **m-AD** in

different mixture of water/THF. (d) Absorption of m-ADA in water/THF mixture. (e) CIE Chromaticity plot of **m-AD** in water/THF showing a single component near-white light emission (0.32, 0.29) at 10% THF/water v/v mixture.

The aggregate induced emission (AIE) property was investigated in dyads **p-AD** and **m-AD** and triad **m-ADA** by measuring fluorescence in solvent mixtures of water and THF. In case of **p-AD**, upon increasing the percentage of water from 90 % to 50 % the overall intensity was decreased, But from 40 % to 10 % water, the fluorescence intensity was almost double than in 40% and it was thrice the value in case of 20% water respectively (Fig. 2.10a). On the other hand, for **m-ADA** the fluorescence intensity increased for 90% and 80% water. Further it uniformly decreased upon increasing percentage of water. A new band around ~ 670 nm was observed due to aggregation upon increasing the water percentage (Fig. 2.10b). In case of **m-AD** it followed the similar behavior as in **p-AD**. It decreased first and from 30% water onwards, the intensity started increasing (Fig. 2.10c). All the dyads and triad formed well-defined nano aggregates (without any agglomeration or precipitation) which restrict the intramolecular rotation resulting in increasing fluorescence intensity. For **p-AD**, the TICT band showed transition towards the LE state (upon decreasing solvent polarity) resulting into slight hypsochromic shift.. The increased fluorescence intensity is attributed to restricted intramolecular rotation and motion in the aggregates that lowered the pathways for non-radiative decay.



**Fig. 2.11** Solutions of **m-ADA** in THF/water v/v left to right: 90/10, 80/20, 70/30, 60/40, 50/50, 30/70, 20/80, 10/90 showing AIE effect.

Interestingly, a chromaticity analysis using International Commission on Illumination (CIE) chromaticity plot for the emission of **m-AD** in all the water/THF solvent mixtures showed emission colors distributed in the blue, green and purple region (figure 2.10d). Remarkably, the solution with 10 % THF and 90 % water showed a near white light emission (Fig 2.10d) with chromaticity coordinates CIE (x, y) of 0.32 and 0.29. The CIE (x, y) chromaticity coordinates of pure white light are 0.33 and 0.33.<sup>6</sup> Such

near white light emission component as well as easily tunable emission in blue, green and purple region are rare to obtain in a single compound and achievable in the present case only through molecular design and by changing solvent compositions.

### **Temperature-induced tunable fluorescence**

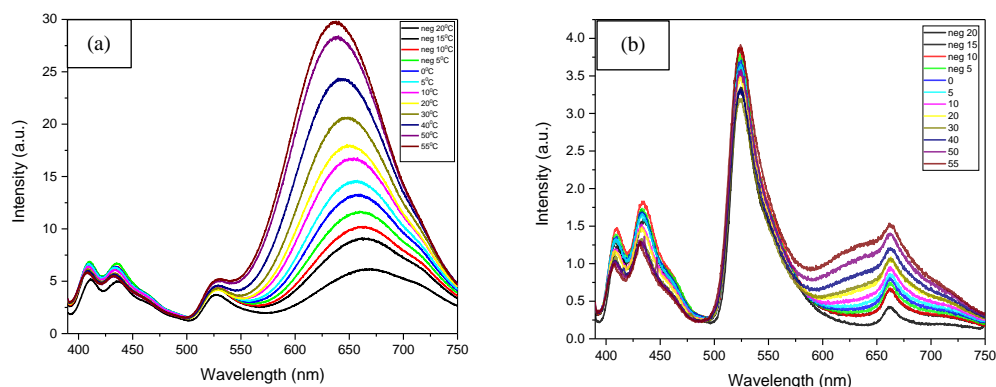


**Fig. 2.12** Emission spectra of (a) **p-AD** and (b) **m-ADA** in chloroform at  $\lambda_{\text{ex}} = 377$  nm and 380 nm respectively.

These kinds of molecular rotors are highly sensitive to temperature and show different emission properties on varying the medium temperature. Temperature sensing in rotor type molecules arises due to two decay channels originating from two molecular conformations (twisted and planar forms) at the excited state. At higher temperatures, faster molecular rotations lead to non-radiative decay and thus decrease in fluorescence intensity. In order to obtain insights about the temperature sensitivity of fluorescence of these dyads and triads, temperature-dependent fluorescence measurements were performed in various solvents.

In **p-AD**, upon decreasing the temperature from 55° C to -20° C in chloroform, a drastic decrease in the fluorescence intensity was observed and it was blue shifted from ~ 670 nm to ~ 636 nm (Fig 2.12a). This is because heating helps in crossing the activation barrier from TICT to the LE state and the LE state gets more populated therefore the value shift and increased intensity. In **m-ADA**, the intensity of the aggregation band (~ 660 nm) was decreased upon decreasing the temperature which is reasonable because decreasing the temperature led to less molecular motion and presumably more aggregation in **m-ADA** resulting in decrease in fluorescence (Fig 2.12b). This trend was not observed for **m-AD** in chloroform. There was no change in peak positions and peak intensity, but in toluene it is changing (Fig 2.13c). So **m-AD** is much lesser temperature

responsive than **p-AD** or **m-ADA**. In other solvents such as toluene, the TICT and the aggregation bands are vanished. Upon decreasing temperature an increase in the fluorescence intensity was observed in all cases (Fig 2.13). Particularly for **p-AD**, temperature dependent fluorescence measurements in three (CF, DCM and THF) out of four different solvents (data in DCM, THF not shown) showed increase in the intensity of the TICT band and a concomitant blue shifting. This is presumably because the higher temperature assists in the crossing of activation barrier from the TICT to LE state and the LE state gets more populated leading to the increase in the band intensity and the blue shift as observed in case of **p-AD**. The effect of temperature of **p-AD** in toluene however was very different as evident from Fig 2.14. In toluene, the TICT band was obviously not present and the spectra showed two bands at 580 nm corresponding to LE state and 530 nm corresponding to the BODIPY emission at low temperature (-25 °C). Upon increasing the temperature, the emission intensity decreased due to enhanced molecular motions and thus opening up of more non-radiative decay channels.

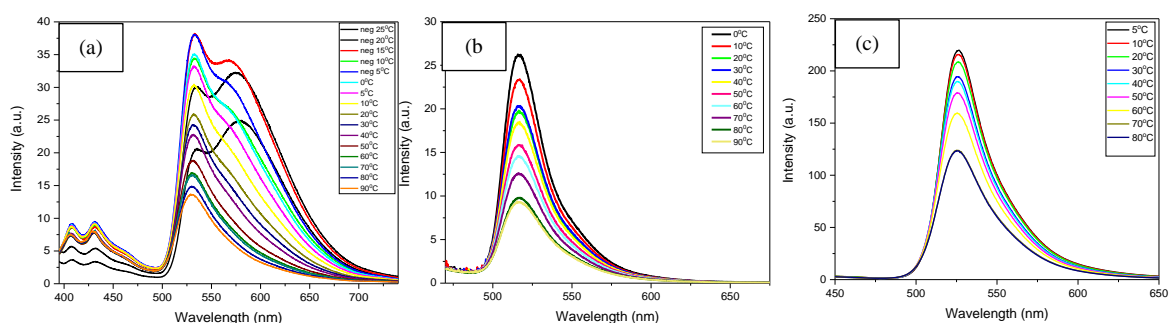


**Fig. 2.13** Emission spectra of (a) **p-AD**, (b) **m-ADA** and (c) **m-AD** in toluene at  $\lambda_{ex} = 377$  nm, 380 nm, 362 nm respectively.

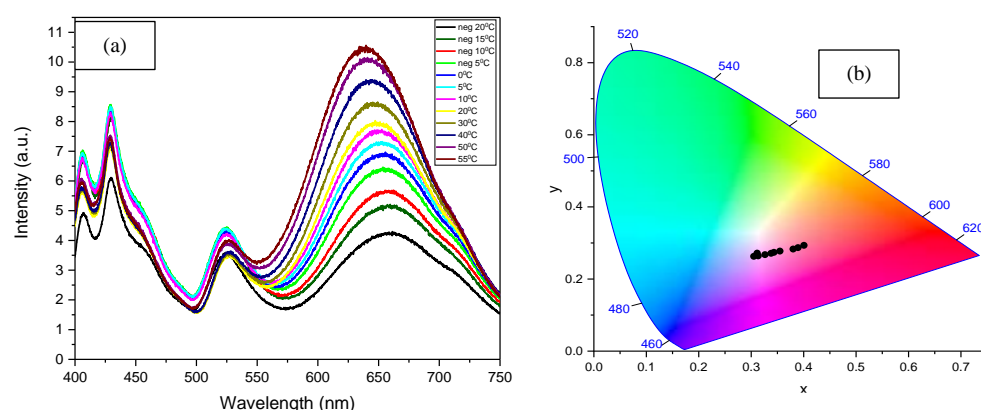


**Fig. 2.14** (a) Emission spectra of **p-AD** in THF at different temperature ( $\lambda_{ex} = 377$  nm). (b) CIE Chromaticity plot of **p-AD** in THF at different temperatures showing a single component near-white light emission for 0 °C, 5 °C and 10 °C.

Fig 2.14a shows the temperature dependent fluorescence of **p-AD** in THF. Interestingly, a chromaticity analysis using International Commission on Illumination (CIE) chromaticity plot for the emission of **p-AD** in THF at different temperatures (-20 °C to 50 °C) showed emission color of near white at three different temperatures (Fig. 2.14b). At temperatures of 0 °C, 5 °C and 10 °C, near white light emission were obtained with chromaticity coordinates CIE (x, y) of (0.33, 0.27), (0.34, 0.27) and (0.35, 0.27) respectively. Such near white light emission component in a single compound at various temperatures is quite rare and justifies the suitability of this compound as a readily tunable fluorescent probe as well as a near white light emitting temperature sensor.

### **Viscosity-induced fluorescence enhancement**

Viscosity dependent emission were measured for dyads **p-AD** and **m-AD** and triad **m-ADA** in a series of solvent mixtures of methanol and glycerol (v/v) to understand the viscosity effect on conformations of these molecules in the excited state.

The fluorescence intensity increases with increasing the viscosity of solvent using a glycerol/methanol mixture. The viscosity was varied from 100/0 to 10/90 methanol/glycerol (0.6 cP to 454 cP) v/v. Restricting the rotation of molecular rotors in a viscous medium enhances fluorescence intensity.

The dielectric constant of methanol and glycerol are 33 and 42 respectively. So the percentage of glycerol is increased there will be an increase in the solvent polarity. The restriction of the intramolecular rotation in a viscous medium hinders the deactivation pathway such as TICT upon increasing the viscosity of the medium and thus the TICT band was completely absent in case of **p-AD** and **m-AD**. In case of **p-AD** the peaks (at ~425 nm and ~520 nm) were neither blue shifted or red shifted upon increasing the percentage of glycerol. But the intensity of the peaks as well as overall shape changed upon increasing percentage of glycerol. One new band formed around ~510 nm which is from the BODIPY emission (Fig 2.15a). Here polarity had no effect because the peak positions did not shift. Only the fluorescence intensity drastically changed (Fig 2.15).

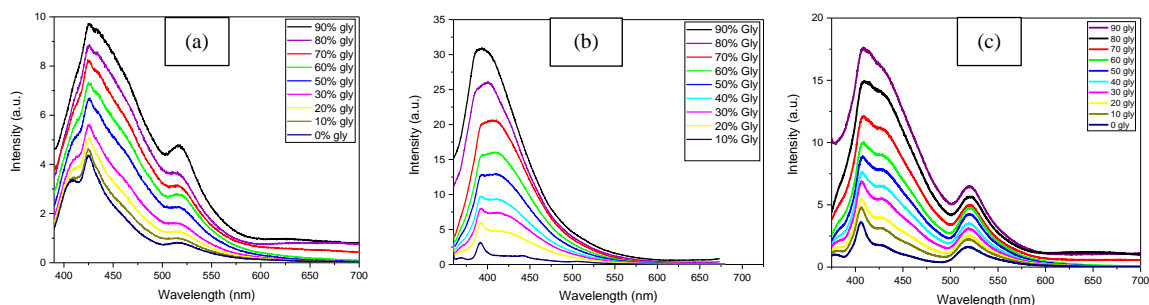


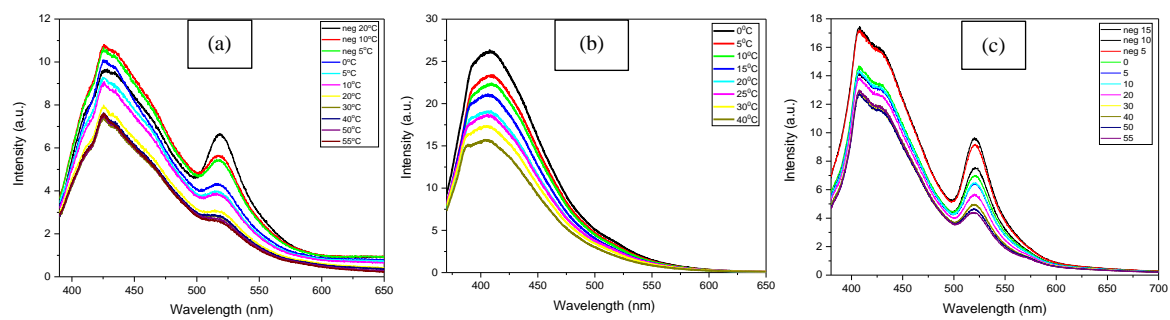
**Fig. 2.15** Emission spectra of (a) **p-AD**, (b) **m-ADA** and (c) **m-AD** in solution of varying viscosities at  $\lambda_{ex} = 377$  nm, 380 nm, 362 nm respectively.

While in **m-ADA** the peaks were slightly blue shifted and the spectra became very broad at 90/10 v/v of glycerol/methanol mixture (Fig. 2.15b). Similar effect was observed in case of **m-AD** where upon increasing the percentage of glycerol, the fluorescence intensity drastically increased 5 times from initial value (Fig. 2.15c). **p-AD** and **m-ADA** showed emission around BDT region that was not changing in terms of peak positions but increased in intensity. Upon increasing the percentage of glycerol, the viscosity of the medium increases that restricts the intramolecular rotation thereby decreasing the non-radiative decay channels and thus enhancing fluorescence intensities, Furthermore, solvent polarity had no effect here and the blue shift observed in **m-ADA** was attributed primarily to the rigidification of the molecular geometry.

### Temperature effect on a particular viscosity

A particular viscous solution of glycerol/methanol mixture 70/30 v/v (104 cP) of **p-AD** and **m-ADA** were taken and temperature dependent fluorescence spectra were recorded. The fluorescence intensity was increased on decreasing the temperature indicating reduced molecular rotations at lower temperatures and thus suppression of non-radiative decay channels (Fig. 2.16). Such temperature effect on variable viscosity of **p-AD** & **m-ADA** are indicative of their potential applications as unique dual temperature & viscosity sensors.



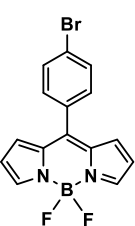
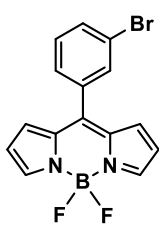
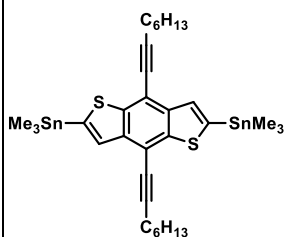
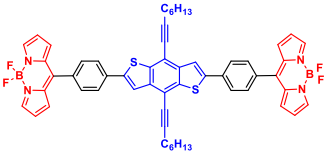
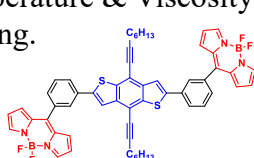
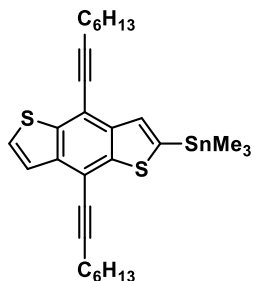
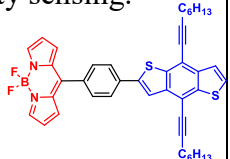
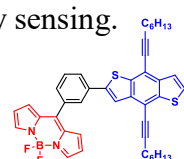


**Fig. 2.16** Fluorescence emission spectra of (a) **p-AD**, (b) **m-ADA** and **m-AD** in glycerol/methanol 70/30 v/v (104 cP) solution

# Chapter 3

## Summary and Outlook

**Table 4.** Summary of the work.

		Acceptors	
			
<b>Donors</b>		<p><b>p-ADA</b></p> <ul style="list-style-type: none"> <li>➤ Remarkable Stokes shift (~194 nm)</li> <li>➤ TICT band (700 nm), Solvatochromism, AIE etc.</li> </ul> 	<p><b>m-ADA</b></p> <ul style="list-style-type: none"> <li>➤ No TICT, but pronounced aggregation.</li> <li>➤ Aggregation evident in UV/VIS and fluorescence in water/THF &amp; Hexane/THF.</li> <li>➤ Shows prominent AIE effect.</li> <li>➤ Temperature &amp; Viscosity sensing.</li> </ul> 
		<p><b>p-AD</b></p> <ul style="list-style-type: none"> <li>➤ High Stokes shift (~149 nm).</li> <li>➤ TICT band (~660 nm).</li> <li>➤ Solvatochromism prominent.</li> <li>➤ AIE is prominent.</li> <li>➤ Shows temperature &amp; viscosity sensing.</li> <li>➤ Dual temperature &amp; viscosity sensing.</li> </ul> 	<p><b>m-AD</b></p> <ul style="list-style-type: none"> <li>➤ Very weak TICT band formation (weaker meta phenyl coupling).</li> <li>➤ Charge transfer is very weak.</li> <li>➤ Solvatochromism is very weak.</li> <li>➤ AIE is present though not so prominent.</li> <li>➤ Reasonable temperature and viscosity sensing.</li> </ul> 

Regioisomeric Triads and Dyads of BDP-BDT were successfully synthesized and characterized by  $^1\text{H}$  NMR,  $^{13}\text{C}$  NMR and mass spectrometry. Their photo physical properties were characterized by optical spectroscopy. **p-AD** shows prominent TICT (~ 150 nm Stokes shift) which is lesser compared to triad counterpart **p-ADA** (~ 194 nm Stokes shift). On comparing dyad regioisomers, **p-AD** shows pronounced TICT and AIE whereas **m-AD** shows negligible TICT owing to weak meta phenyl coupling. On comparing triad regioisomers, **p-ADA** shows TICT, AIE whereas **m-ADA** shows aggregation. All dyads and triads show distinct temperature dependent emission and thus are potential “**molecular thermometers**” that can be used for microenvironment temperature sensing and show viscosity induced fluorescence enhancement and are potential “**viscosity sensors**” and also dual temperature and viscosity sensors.

# Chapter 4

## Experimental section

### General information:

#### 4.1 Materials

All the reagents and solvents were purchased from Sigma Aldrich, Merck, and Himedia. Solvents such as dichloromethane (DCM) were distilled using standard distillation setup, where toluene was dried using Mbraun MB-SPS solvent drying unit. Tetrahydrofuran (THF) was dried over sodium/benzophenone and distilled prior to use. DCM was dried over phosphorus pentoxide and distilled prior to use. DMF was dried over calcium sulphate and distilled under reduced pressure prior to use. Preparatory TLC used for purification is made up of silica gel G 500 micron. Silica gel of mesh size 60-120 was used for column chromatography. Solvents used for column chromatography and extraction (such as hexane, DCM, chloroform and ethyl acetate) were directly used without any further distillation. Reactions were monitored in thin layer chromatography (TLC) plates on silica gel and visualized under UV lamp (254 and 365 nm).

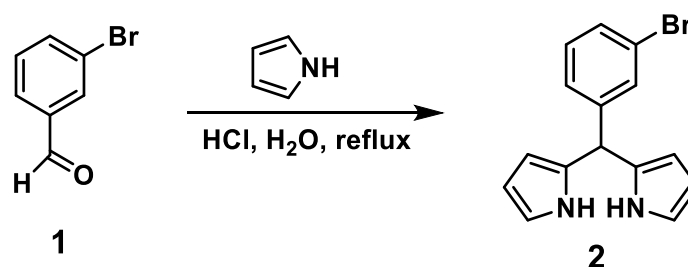
#### 4.2 Measurements

The  $^1\text{H}$  and  $^{13}\text{C}$  NMR spectra were recorded on a 400 MHz Bruker Biospin Avance III FT-NMR spectrometer, respectively with TMS as standard at room temperature. The solvents used were  $\text{CDCl}_3$  and  $\text{DMSO-d}_6$ . Column chromatography was done with silica gel (100-200) mesh size. Mass spectra was recorded in both ESI positive and negative modes using Waters SYNAPT G2S High Definition HRMS mass spectrometer. UV-Vis was recorded on PerkinElmer LAMBDA 365 UV/Vis spectrophotometer, using a thermo stated quartz cuvette with 1 mm path length at 25  $^\circ\text{C}$ . Fluorescence solution measurements were performed with Hitachi F7000 fluorescence spectrophotometer. The spectrometer was equipped with R928F photomultiplier expandable up to 900 nm. Standard software FL Solutions was used for the measurement and analysis of the data. Various excitation wavelengths were used to perform the fluorescence measurements. Temperature dependent fluorescence measurements were performed with the same

spectrophotometer equipped with Peltier system from Newport, USA with a temperature range of -20 °C to 100 °C.

### 4.3 Synthesis

#### 4.3.1 Synthesis of 2,2'-((3-bromophenyl)methylene)bis(1H-pyrrole)

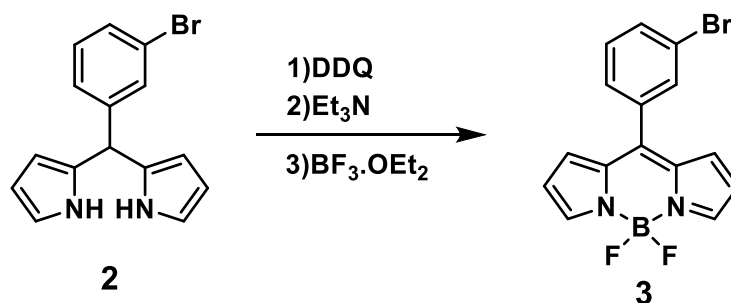


**Scheme 4.1.** Synthesis of dipyrromethane (DPM).<sup>13</sup>

A solution of 3-bromobenzaldehyde (1.0 g, 5.4048 mmol) in pyrrole (1.87 ml, 27.0240 mmol) was refluxed at 100 °C, in the presence of H<sub>2</sub>O (12 mL) and HCl (36.5 wt.%, 40 μL), for 1 hour. The product formed was extracted using ethyl acetate and then the solvent was evaporated in vacuum using a rotary evaporator. The resulting reaction mixture was then subjected to column chromatography with petroleum ether/ethyl acetate (90/10 v/v) as the eluent. The resulting compound dipyrromethane was a brown oil obtained with a yield of 43%.

**<sup>1</sup>H NMR (400 MHz, CDCl<sub>3</sub>):** 8.04 (s, 2 H), 7.39-7.36 (m, 2 H), 7.20-7.12 (m, 2 H), 6.71-6.70 (m, 2 H), 6.17-6.14 (q, 2 H), 5.90-5.89 (q, 2 H), 5.4 (s, 1 H).

#### 4.3.2 Synthesis of acceptor (Meta substituted BODIPY)

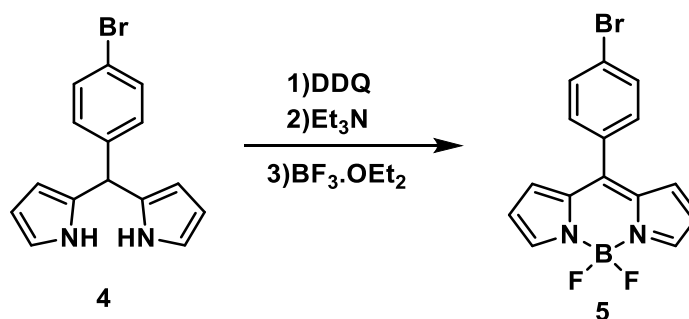


**Scheme 4.2.** Synthesis of acceptor m-BODIPY-Br.<sup>13</sup>

Dipyrromethane **2** (0.715 g, 2.3739 mmol) was dissolved in 20 mL dry dichloromethane (DCM) and to that, 2, 3-Dichloro-5, 6-dicyano-1, 4-benzoquinone (DDQ) (0.65g, 2.8634 mmol) was added. Subsequently, triethylamine (3.7 mL) was added to the reaction mixture after 3 hours and  $\text{BF}_3 \cdot \text{OEt}_2$  (3.7 mL) was added after 6 hours and the reaction mixture was stirred overnight. The reaction mixture was filtered through a silica gel column with DCM as solvent to remove the DDQ. The resulting reaction mixture was extracted with DCM and the aqueous layer was neutralized with saturated  $\text{NaHCO}_3$  solution and organic layer washed several times with saturated brine solution. The organic layer was dried over  $\text{Na}_2\text{SO}_4$  and solvent was removed with rotary evaporator. The crude product obtained was subjected to silica gel column chromatography and ethyl acetate / hexane (10/90 v/v) as eluent to obtain the BODIPY compound **3** as orange solid powder with a yield of 19% yield.

$^1\text{H NMR}$  (400MHz,  $\text{CDCl}_3$ ): 7.96 (s, 2 H), 7.72 (d, J = 8 Hz, 2 H), 7.50 (d, J = 8 Hz, 1 H), 7.41 (t, J = 8 Hz, 1 H), 6.92 (d, J = 4 Hz, 2 H), 6.57 (d, J = 4 Hz, 2 H).

#### 4.3.3 Synthesis of acceptor (Para substituted BODIPY)



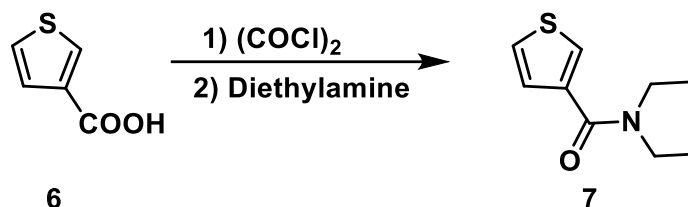
**Scheme 4.3.** Synthesis of acceptor p-BODIPY-Br.<sup>13</sup>

Dipyrromethane (DPM) **4** was prepared from 4-bromobenzaldehyde using the same method mentioned for Meta substituted dipyrromethane above. DPM **4** (0.200 g, 0.6640 mmol) was dissolved in 10 mL dry dichloromethane (DCM) and to that; DDQ (0.182 g, 0.8027 mmol) was added. Subsequently, triethylamine (1 mL) was added to the reaction mixture after 3 hours and after further 4 hours,  $\text{BF}_3 \cdot \text{OEt}_2$  (1 mL) was added and the reaction mixture was stirred overnight. The reaction mixture was filtered through a silica gel column with DCM as solvent to remove the DDQ. The resulting reaction mixture was extracted with DCM and the aqueous layer was neutralized with saturated  $\text{NaHCO}_3$

solution and organic layer washed with saturated brine solution. The organic layer was dried over sodium sulphate and solvent was removed with the rotary evaporator. The crude product obtained was subjected to silica gel column chromatography and ethyl acetate / hexane (5/95 v/v) as eluent which resulted in orange solid compound and the yield was 69%.

**<sup>1</sup>H NMR (400MHz, CDCl<sub>3</sub>):** 7.96 (s, 2 H), 7.68 (d, J = 8 Hz, 2 H), 7.45 (d, J = 8 Hz, 2 H), 6.91 (d, J = 4 Hz, 2 H), 6.57 (d, J = 4 Hz, 2 H).

#### 4.3.4 Synthesis of (N,N-diethyl)thiophenecarboxylamide

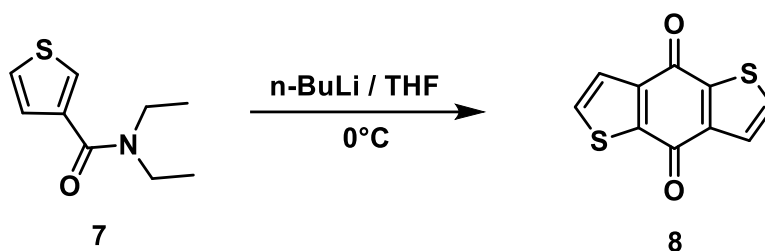


**Scheme 4.4.** Synthesis of (N,N-diethyl)thiophenecarboxylamide.<sup>15</sup>

2 g (15.6057 mmol) of thiophene-3-carboxylic acid was added to 15 mL of dichloromethane taken in a round bottomed flask fitted with CaCl<sub>2</sub> guard tube. The solution was cooled on an ice bath and 7.92 g (62.4228 mmol) of oxalyl chloride was added dropwise. The reaction mixture was stirred at room temperature for overnight. The excess oxalyl chloride was removed under vacuum. The acyl chloride intermediate was dissolved in 10 mL of dry dichloromethane. The solution of acid chloride was then added dropwise to the solution containing diethylamine 3.2 g (43.7517 mmol) in 30mL of dry dichloromethane in a two necked round bottomed flask fitted with a CaCl<sub>2</sub> guard tube and cooled on an ice bath. The reaction mixture was stirred for 3 hours at room temperature and washed with water. The organic fraction was dried using anhydrous sodium sulphate, solvent evaporated and purified by silica gel column chromatography using ethyl acetate/ hexane (30/70 v/v) mixture as eluent. Pure product was obtained as colorless oily liquid with a yield of 97%.

**<sup>1</sup>H NMR (400MHz, CDCl<sub>3</sub>):** 7.47-7.32 (m, 1 H), 7.31 (d, J = 4Hz, 1 H), 7.18 (d, J = 4 Hz, 1 H), 3.52-3.37 (m, 4 H), 1.24-1.19 (d, J = 20 Hz, 6 H).

#### 4.3.5 Synthesis of Benzo[1,2-b:4,5-b']dithiophene-4,8-dione

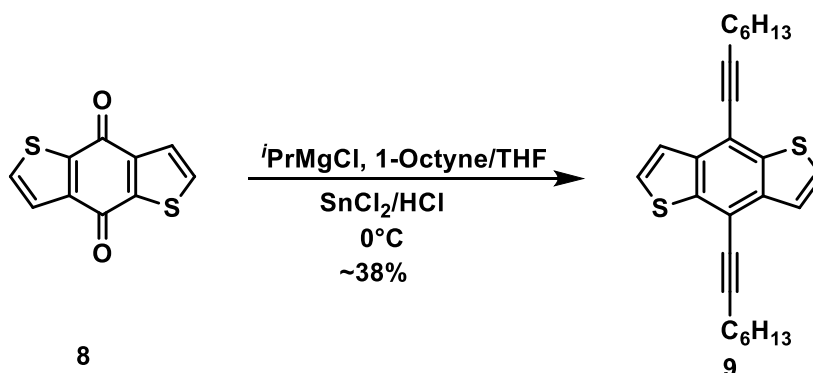


Scheme 4.5. Synthesis of BDT-dione.<sup>15</sup>

Compound 7 (1.308 g, 7.1362 mmol) was dissolved in distilled THF. Then the solution was cooled to  $0^\circ\text{C}$  and 6.11 mL of  $n\text{-BuLi}$  (1.6M in hexane) was added dropwise while stirring under inert atmosphere. The solution was stirred at room temperature for 3 hours and later it was poured into a beaker which contained ice-water. Yellowish precipitate formed immediately and the mixture was stirred overnight. The precipitate was filtered out using Buchner apparatus and washed with water, methanol and hexane successively and dried under vacuum. 0.435 g (27 %) of yellow solid was obtained as product.

$^1\text{H NMR}$  (400MHz,  $\text{CDCl}_3$ ): 7.69 (d,  $J = 4$  Hz, 2 H), 7.65 (d,  $J = 4$  Hz, 2 H).

#### 4.3.6 Synthesis of 4,8-Di(oct-1-yn-1-yl)benzo[1,2-b:4,5-b']dithiophene



Scheme 4.6. Synthesis of alkylated Benzodithiophene.<sup>15</sup>

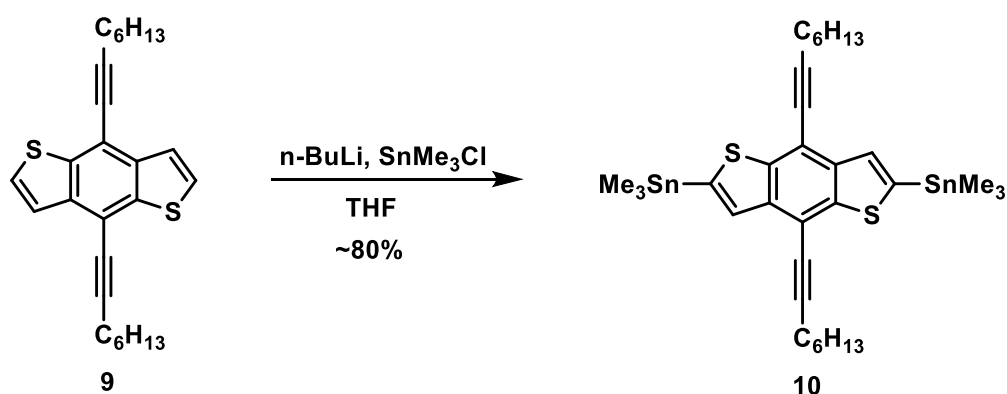
Isopropylmagnesium chloride (2 M in THF, 1.2 mL, 2.3971 mmol) was added dropwise to 1-octyne (0.29 g, 2.6315 mmol) at  $0^\circ\text{C}$ . Then the reaction mixture was heated to  $60^\circ\text{C}$  and stirred for 100 min. It was cooled to RT, and benzo [1,2-b:4,5-b']dithiophene-4,8-dione (100 mg, 0.4540 mmol) was added (which was already degassed with 5-6 freeze-



pump-thaw cycles). Again it was heated upto 60 °C and stirred for 120 min. It was then cooled to RT, and 0.7 g of SnCl<sub>2</sub> in HCl solution (16 mL, 10%) was added dropwise to the reaction mixture. The reaction mixture was heated at 65 °C for 60 min, then cooled down to room temperature, and poured into water and extracted with hexane twice. The organic fraction was dried over anhydrous Na<sub>2</sub>SO<sub>4</sub> and concentrated under vacuum. Light yellow solid product was obtained by recrystallization of the crude from ethanol with a yield of 38%.

<sup>1</sup>H NMR (400MHz, CDCl<sub>3</sub>): 7.57 (d, J = 8 Hz, 2 H), 7.50 (d, J = 4 Hz, 2 H), 2.63 (t, J = 8 Hz, 4 H), 1.73-1.68 (m, 4 H), 1.38-1.25 (m, 12 H), 0.94-0.86 (m, 6 H).

#### 4.3.7 Synthesis of donor (4,8-di(oct-1-yn-1-yl)benzo[1,2-b:4,5-b']dithiophene-2,6-diyl) bis(trimethylstannane)

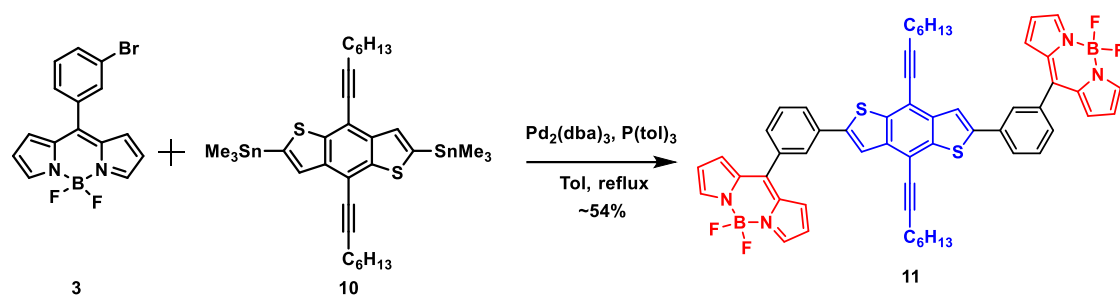


**Scheme 4.7.** Synthesis of Donor.<sup>15</sup>

200 mg (0.49 mmol) of **4** was dissolved in dry THF. The solution was cooled to -78 °C and 1.2 mL (1.97 mmol) of *n*-BuLi (1.6 M solution in hexane) was added drop wise while stirring under inert atmosphere and the reaction mixture was stirred at -78°C for 1 h which was followed by addition of 1.97 mL (1.97 mmol) of trimethyltin chloride (1 M solution in hexane). The reaction mixture was stirred overnight at room temperature. The reaction was quenched by adding water and extracted with diethyl ether. Compound **10** was obtained as yellow crystalline solid upon recrystallization from ethanol solution of the crude product with a yield of 80%.

<sup>1</sup>H NMR (400MHz, CDCl<sub>3</sub>): 7.61 (s, 2 H), 2.65 (t, J = 6.8 Hz, 4 H), 1.72-1.53 (m, 18 H), 0.95-0.92 (m, 6 H), 0.45 (t, J = 28 Hz, 18 H)

#### 4.3.8 Synthesis of m-ADA triad using Stille coupling reaction

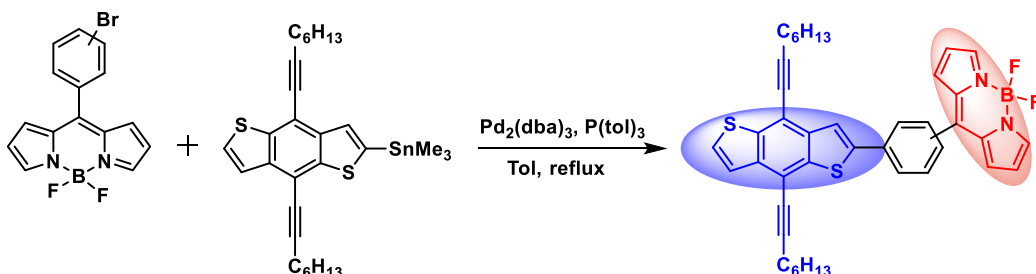


**Scheme 4.8.** Stille coupling of acceptor and donor to form triad m-ADA.<sup>13</sup>

Compound **3** (50 mg, 0.1385 mmol) was dissolved in dry toluene (25 mL) and solution was degassed using Freeze-Pump-Thaw method. Then, distannylated BDT compound **10** (51 mg, 0.0692 mmol) was added, which was already degassed with the mentioned method and the solution was stirred under argon.  $\text{Pd}_2(\text{dba})_3$  (2.5 mg, 0.0027 mmol) and  $\text{P}(\text{o-tol})_3$  (3.9 mg, 0.1605 mmol) were added and then refluxed for 3 h. The reaction mixture was cooled to RT and subsequently the solvent was evaporated on rotary evaporator. Further, the reaction mixture was subjected to column chromatography purification using DCM/petroleum ether (50/50 v/v) resulting in isolation of reddish solid compound with yield of 54 %.

**<sup>1</sup>H NMR (400MHz, CDCl<sub>3</sub>):** 7.99-7.96 (d, *J*= 12 Hz, 8 H), 7.84 (s, 2 H), 7.64-7.60 (t, *J*= 8 Hz, 2 H), 7.56 (d, *J*= 4 Hz, 2 H), 7.02 (d, *J*= 4 Hz, 4 H), 6.60 (d, *J*= 4 Hz, 4 H), 2.68-2.64 (t, *J*= 8 Hz, 4 H), 1.75-1.73 (m, 4 H), 1.36-1.34 (m, 12 H), 0.90-0.87 (m, 6 H).

#### 4.3.9 General synthesis scheme of Control compounds m-AD and p-AD using Stille coupling reaction



**Scheme 4.9.** Synthesis of m-AD and p-AD compounds using Stille coupling.<sup>13</sup>

Compound **3** or **5** (50 mg, 0.1385 mmol) was dissolved in dry toluene (25 mL) and solution was degassed for 6 cycles using freeze-pump-thaw method. Then a mixture of

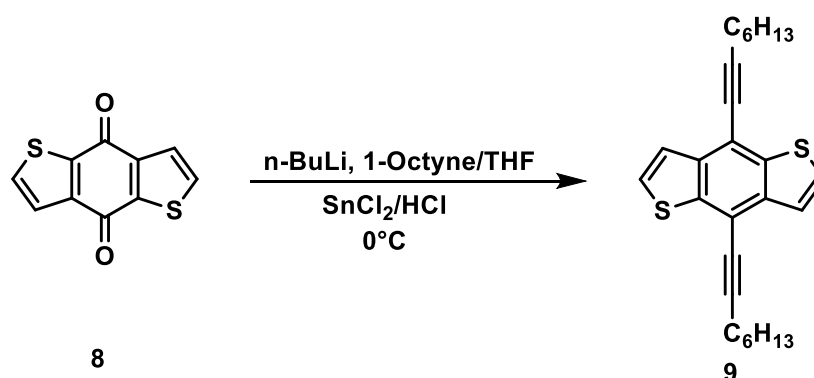
monostannylated and distannylated BDT compound (51 mg, 0.0692 mmol) was added, which was already degassed with above mentioned method. Pd<sub>2</sub>(dba)<sub>3</sub> (2.5 mg, 0.0027 mmol) and P(o-tol)<sub>3</sub> (3.9 mg, 0.1605 mmol) were added and the reaction mixture was purged for another 15 min and then refluxed for 4 h. The reaction mixture was cooled to RT and the solvent was evaporated on rotary evaporator. Subsequently it was purified using preparatory TLC plates using ethyl acetate/hexane (20/80 v/v) as eluent, resulting in isolation of orange solid compounds with yield of 14% and 11% for **m-AD** and **p-AD** respectively.

**m-AD (12)** <sup>1</sup>H NMR (400MHz, CDCl<sub>3</sub>): 7.97 (d, J = 12 Hz, 4H), 7.85 (s, 1 H), 7.61-7.51 (m, 4H), 7.01 (d, J = 4 Hz, 2H), 6.58 (d, J = 4 Hz, 2H), 2.67-2.62 (m, 4 H), 1.77-1.70 (m, 4 H), 1.37-1.33 (m, 12 H), 0.91-0.88 (m, 6H). **ESI-TOF** : (M+H)<sup>+</sup> of molecular formula C<sub>41</sub>H<sub>39</sub>BF<sub>2</sub>N<sub>2</sub>S<sub>2</sub> : Calculated 673.2694 ; found 673.3224.

**p-AD (13)** <sup>1</sup>H NMR (400MHz, CDCl<sub>3</sub>): 7.97-7.93 (t, J = 8 Hz, 5H), 7.67 (d, J = 8Hz, 2H), 7.58 (d, J = 4Hz, 2H), 7.53 (d, J = 4Hz, 2 H), 7.02 (d, J = 4Hz, 2 H), 6.58 (d, J = 4Hz, 2 H), 2.69-2.65 (m, 4 H), 1.78-1.75 (m, 4 H), 1.39 (d, J = 4 Hz, 12 H), 0.89-0.86 (t, J = 4 Hz, 6H). **ESI-TOF** : (M+H)<sup>+</sup> of molecular formula C<sub>41</sub>H<sub>39</sub>BF<sub>2</sub>N<sub>2</sub>S<sub>2</sub> : Calculated 673.2694 ; found 673.3917

#### 4.4 Some trial reactions for preparation of Alkylated BDT:

##### 4.4.1 Synthesis of 4,8-Di(oct-1-yn-1-yl)benzo[1,2-b:4,5-b']dithiophene using n-BuLi

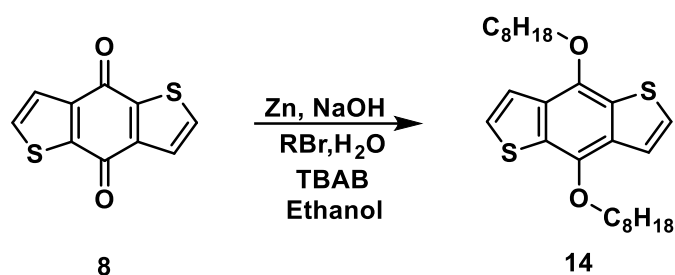


**Scheme 4.10.** Synthesis of alkylated BDT with n-BuLi as base.<sup>15</sup>

n-BuLi (2 M solution, 1.2 mL, 2.3971 mmol) was added dropwise to a solution of 1-octyne (0.290 g, 2.6315 mmol) at 0 °C. The reaction mixture was heated up to 60 °C and stirred for 100 min. It was cooled to RT, and benzo[1,2-b:4,5-b']dithiophene-4,8-dione (100 mg, 0.4540 mmol) was added. The reaction mixture was heated up to 60°C and

stirred for 120 min. It was then cooled to RT, and 0.7 g of SnCl<sub>2</sub> in HCl solution (16 mL 10%) was added dropwise to the reaction mixture. The reaction mixture was heated at 65 °C for 60 min, then cooled down to room temperature, and poured into 100 mL of water. It was extracted with 50 mL of hexane twice. However in this case, reaction didn't proceed, only starting material remained in the reaction.

#### 4.4.2 Synthesis of 8-bis((2-ethylhexyl)oxy)benzo[1,2-b:4,5-b']dithiophene



**Scheme 4.11.** Synthesis of compound 14. <sup>16</sup>

Benzodithiophene was mixed with Zn powder (130 mg, 1.9883 mmol) and NaOH (10 mL, 25 wt%) solution under nitrogen. The resulting mixture was refluxed for 2 hours. Then ethyl hexyl bromide (0.484 mL, 2.7236 mmol) and catalytic amount of TBAB were sequentially added into the solution. After being refluxed for overnight, the reaction mixture was poured into cold water and extracted with diethyl ether. The collected organic layers were dried over Na<sub>2</sub>SO<sub>4</sub> and concentrated under vacuum. Product was purified using pure hexane as eluent which yielded colorless oil with very low yield.

**Since the yield was very low for the above reaction, several other reaction conditions were tried in order to standardize the synthesis.**

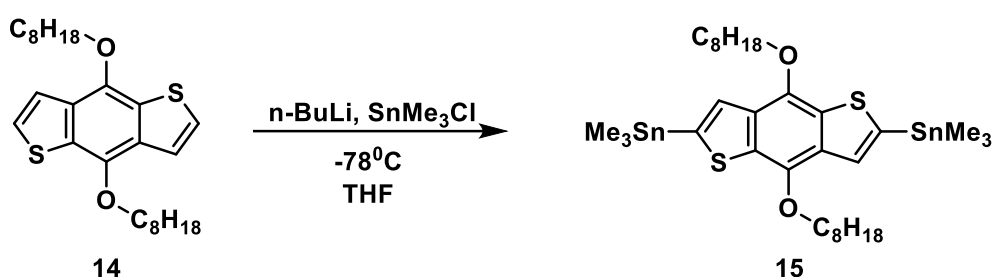
**Table 4 :** Various standardization methods to prepare 8-bis((2-ethylhexyl)oxy)benzo[1,2-b:4,5-b']dithiophene.

Reagents (order in which the reagents are added)	Solvent	Detail of reagents added	Result
BDT+Zn+NaOH+RBr+TBAB	H <sub>2</sub> O	25 wt% NaOH	Starting material (SM) was major, Product formed (3 spots) , 2 spots above SM.
BDT+Zn+NaOH+RBr	H <sub>2</sub> O	15 wt% NaOH	Same as previous reaction, but

+TBAB			one more spot below SM.
BDT+Zn+NaOH+RBr +TBAB	H <sub>2</sub> O, EtOH	13 wt% NaOH	SM was major, but better than previous reaction.
BDT+Zn+H <sub>2</sub> O+NaOH +EtOH+RBr+TBAB	H <sub>2</sub> O, EtOH	18 wt% NaOH Zn added in two parts. NaOH added directly.	No SM. Only two spots above SM. Color change also observed.
BDT+Zn+H <sub>2</sub> O+NaOH +EtOH+RBr+TBAB	H <sub>2</sub> O, EtOH	23 wt% NaOH Zn added in two parts. NaOH added directly.	Only SM. No color change.
BDT+Zn+H <sub>2</sub> O+NaOH +EtOH+RBr+TBAB	H <sub>2</sub> O, EtOH	18 wt % NaOH Zn added in two parts. NaOH added directly.	Only SM. No color change.
BDT+Zn+H <sub>2</sub> O+NaOH +EtOH+RBr+TBAB	H <sub>2</sub> O, EtOH	18wt% NaOH Zn added in two parts. NaOH added directly. More ethanol was added.	SM was major. Yield was very low.
BDT+Zn+H <sub>2</sub> O+NaOH +EtOH+RBr+TBAB	H <sub>2</sub> O, EtOH	18 wt% NaOH Zn added in two parts. NaOH added directly. More ethanol is added.	SM was major. Yield was low. No color change was observed. (Dark red throughout the reaction)
BDT+Zn+NaOH+ TBAB+RBr	H <sub>2</sub> O	18 wt% NaOH No ethanol. Zn added in one part. More RBr was used. Order in which the reactants are added different from previous reaction.	No reaction Only SM.

BDT+Zn+EtOH+ NaOH+RBr+TBAB	EtOH	18 wt% NaOH Only ethanol as solvent. Purged the reagents before reaction. Zn added in two parts	No reaction. Only SM. No color change. Dark red throughout the reaction.
-------------------------------	------	--	--

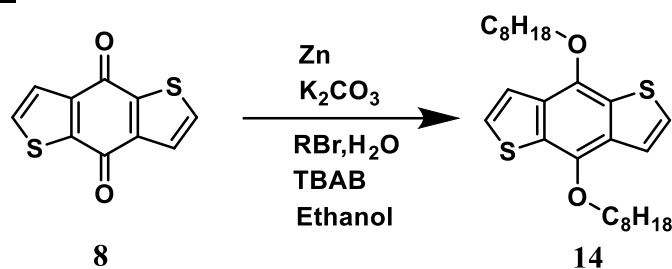
#### 4.4.3 Synthesis of 8-bis((2-ethylhexyl)oxy)benzo[1,2-b:4,5-b']dithiophene-2,6-diyl) bis(trimethylstannane)



**Scheme 4.12.** Synthesis of 8-bis((2-ethylhexyl)oxy)benzo[1,2-b:4,5-b']dithiophene-2,6-diyl) bis(trimethylstannane).<sup>16</sup>

20 mg (0.0447 mmol) of compound **14** was dissolved in dry THF and the solution was cooled to  $-78^{\circ}\text{C}$  and 0.0564 mL of *n*-BuLi (2 M solution in hexane) (0.1128 mmol) was added dropwise while stirring under inert atmosphere. The reaction mixture was stirred at  $-78^{\circ}\text{C}$  for 1 hour following which 135  $\mu\text{L}$  of Trimethyltin chloride (1 M solution in hexane) (0.1352 mmol) was added to it. The reaction mixture was stirred overnight at room temperature. The reaction was quenched by adding water and extracted with diethyl ether. TLC was checked after the reaction in pure hexane, Only one product was formed in the reaction which was highly non-polar. **15** was obtained as colorless crystalline solid after concentrating using vacuum. But, from the analysis of the  $^1\text{H}$  NMR, the  $\text{SnMe}_3$  peaks were missing. Thus the reaction failed.

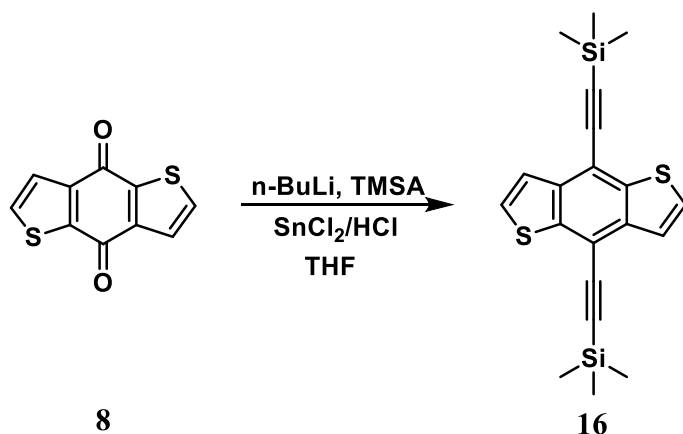
#### 4.4.4 Synthesis of 8-bis((2-ethylhexyl)oxy)benzo[1,2-b:4,5-b']dithiophene using mild base



**Scheme 4.13.** Synthesis of Compound 14 using a mild base  $K_2CO_3$ .<sup>16</sup>

Benzodithiophene-dione **8** was mixed with Zn powder (20.77 mg, 0.3178 mmol) and  $K_2CO_3$  (44 mg, 0.3178 mmol) and water-ethanol mixture added under nitrogen. The resulting mixture was refluxed for 2 hours. Then ethylhexyl bromide and catalytic amount of TBAB were sequentially added into the solution. After being refluxed for overnight, the reaction mixture was poured into cold water and extracted with diethyl ether. Only starting material remained in the reaction, product didn't form.

#### 4.4.5 Synthesis of 4,8-bis(triisopropylsilylethynyl)benzo[1,2-b:4,5-b']dithiophene



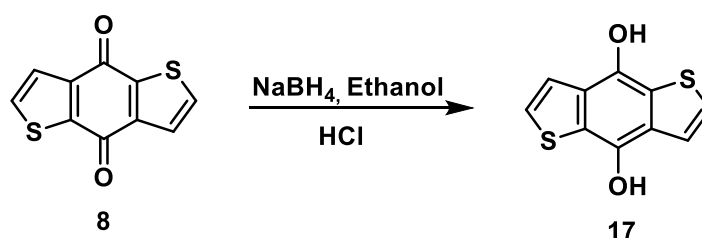
**Scheme 4.14.** Synthesis of 4,8-bis(triisopropylsilylethynyl)benzo[1,2-b:4,5-b']dithiophene.<sup>17</sup>

In a 50 mL flask under inert atmosphere, (trimethylsilyl)acetylene (0.3 mL, 1.3541 mmol) was dissolved in dry THF (20 mL). A solution of n-butyllithium (1.6 M in hexane, 0.68 mL, 1.3620 mmol) was added dropwise. After stirring for 20 min, a suspension of benzodithiophene-4,8-dione (100 mg, 0.4540 mmol) in dry THF (2 mL) was added rapidly to the reaction mixture. Subsequently, the reaction mixture was heated to 50 °C and stirred for 1 hour. After cooling down to room temperature, a solution of tin(II)-

chloride dihydrate (0.419 g, 1.816 mmol) in 32% hydrochloric acid (2 mL) was added, and the resulting mixture was vigorously stirred at room temperature for 1 hour. After addition of diethyl ether (50 mL), the organic layer was separated, washed with water and saturated brine solution, organic layers collected and dried over Na<sub>2</sub>SO<sub>4</sub>. The crude product was purified by column chromatography by using hexane as eluent by silica gel column chromatography to afford **16** as a colorless crystalline solid with a yield of 45%.

<sup>1</sup>H NMR (400MHz, CDCl<sub>3</sub>): 7.60 (d, J= 4 Hz, 2 H), 7.55 (d, J= 4 Hz, 2 H), 0.36 (s, 18 H)

#### 4.4.6 Synthesis of 4,8-Dihydroxybenzo[1,2-b:4,5-b']dithiophene from dione **8**



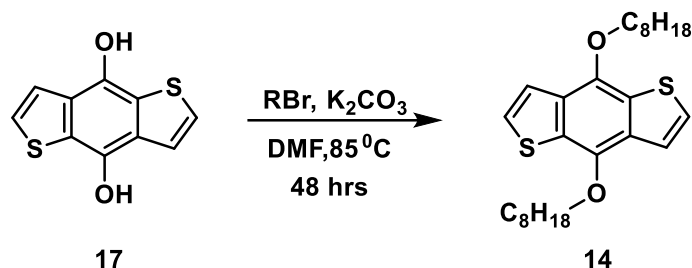
**Scheme 4.15.** Synthesis procedure for benzo[1,2-b:4,5-b']dithiophene-4,8-diol from benzo[1,2-b:4,5-b']dithiophene-4,8-dione.<sup>18</sup>

To a stirred suspension of compound **8** (100 mg, 0.4540 mmol) in 10 mL of ethanol was added to NaBH<sub>4</sub> (0.686 g, 1.8157 mmol) in portion-wise at 0 °C. This was followed by stirring for 5 h at room temperature. Then the reaction was quenched by pouring it into 1 M HCl. The crude product was filtered, washed with large amounts of water, and dried under vacuum at 70 °C. The product was obtained as a green solid with a yield of 85% and used for next step without further purification. Product was characterized using FTIR spectroscopy. The –OH stretch was found around 3276.98 Cm<sup>-1</sup>.

<sup>1</sup>H NMR (400MHz, DMSO): 9.80 (s, 2 H), 7.62 (d, J= 4 Hz, 2 H), 7.56 (d, J= 4 Hz, 2 H).



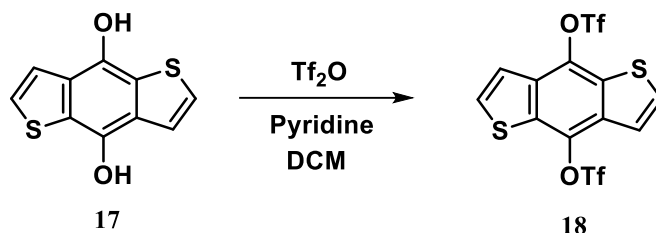
#### 4.4.7 Synthesis of 8-bis((2-ethylhexyl)oxy)benzo[1,2-b:4,5-b']dithiophene using DMF as solvent



**Scheme 4.16.** Synthesis of compound 12 using DMF as solvent.<sup>18</sup>

Benzo[1,2-b:4,5-b']dithiophene-4,8-diol (**6**) (0.03 g, 0.1351 mmol), Ethylhexyl bromide (0.078 g, 0.4053 mmol), K<sub>2</sub>CO<sub>3</sub> (0.187 g, 1.3530 mmol) and DMF/CH<sub>3</sub>CN (15 mL) were mixed together. The mixture was refluxed at 85 °C and stirred for 48 h, then it was cooled to room temperature, filtered and the solvent was removed under vacuum. The residue was dissolved in CH<sub>2</sub>Cl<sub>2</sub> and washed with H<sub>2</sub>O. Then the organic phase was dried over anhydrous Na<sub>2</sub>SO<sub>4</sub> and the solvent was removed under vacuum. Starting material remained in the reaction. Reaction didn't work in this case.

#### 4.4.8 Synthesis of 4,8-Bis(trifluoromethanesulfonyloxy)benzo[1,2-b:4,5-b']dithiophene



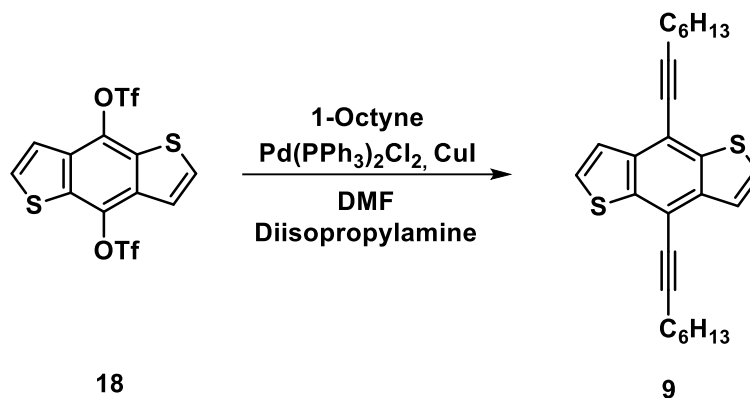
**Scheme 4.17** Synthesis of 4,8-Bis(trifluoromethanesulfonyloxy)benzo[1,2-b:4,5-b']dithiophene.<sup>19</sup>

Trifluoromethanesulfonic anhydride (0.113 mL, 0.294 mmol) was added to the suspension of **17** (0.05 g, 0.225 mmol) and dry pyridine (0.05 mL) in dichloromethane (30 mL) at 0 °C. After the mixture was stirred at 0 °C for 12 h, water and hydrochloric acid (1 M) were added. The resulting mixture was extracted with dichloromethane, and the combined organic layer was dried (Na<sub>2</sub>SO<sub>4</sub>) and concentrated in vacuum. The residue was purified with column chromatography on silica gel eluted with petroleum ether/ethylacetate (80:20 v/v) to obtain compound **18** as white solid with a yield of 12%.

Formation of bistriflate **16** was confirmed from the NMR (protons from –OH peaks were missing).

$^1\text{H}$  NMR (400MHz,  $\text{CDCl}_3$ ): 7.68 (d,  $J = 4$  Hz, 2 H), 7.57 (d,  $J = 4$  Hz, 2 H).

#### 4.4.9 Palladium-catalyzed Sonogashira coupling of bistriflate **16** with terminal alkyne



**Scheme 4.18** Synthesis of 4,8-di(oct-1-yn-1-yl)benzo[1,2-b:4,5-b']dithiophene. <sup>19</sup>

The bistriflate **18** (8 mg, 0.0164 mmol), 1-octyne (0.0478 mmol) and  $\text{Pd}(\text{PPh}_3)_2\text{Cl}_2$  (2.28 mg, 0.0015 mmol, 10 mol %),  $\text{CuI}$  (1.2 mg, 0.0062 mmol, 20 mol% equiv.) were placed in a round-bottomed flask, fitted with a condenser, under nitrogen.  $\text{DMF}$  (4 mL) and diisopropylamine (4 mL) was added to that and the mixture was stirred for 12 h at 100 °C then poured onto aqueous hydrochloric acid (1 mL, 1 M) and was concentrated using vacuum. Reaction ended up in many side products and their separation seemed difficult and moreover, the crude NMR did not show any aromatic protons.

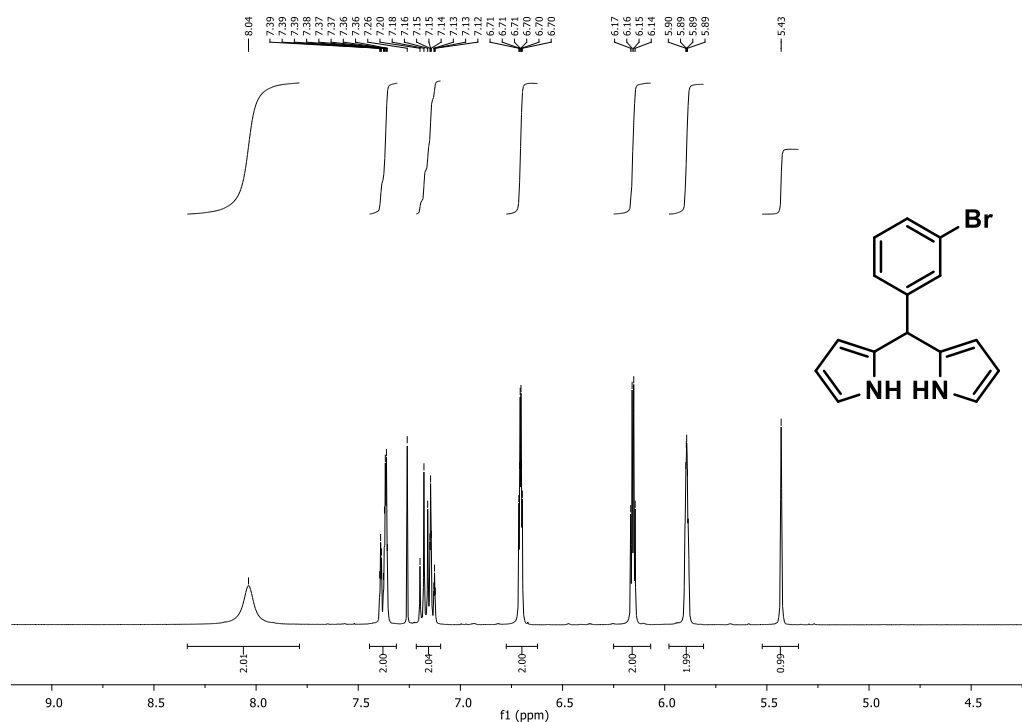
# References

- (1) Ni, Y.; Wu, J., *Org. Biomol. Chem.* **2014**, *12* (23), 3774–3791.
- (2) Cheng, M. H. Y.; Savoie, H.; Bryden, F.; Boyle, R. W., *Photochem. Photobiol. Sci.* **2017**, *16* (8), 1260–1267.
- (3) Huo, L.; Hou, J., *Polym. Chem.* **2011**, *2* (11), 2453–2461.
- (4) Sasaki, S.; Drummen, G. P. C.; Konishi, G. I., *J. Mater. Chem. C* **2016**, *4* (14), 2731–2743.
- (5) Cao, C.; Liu, X.; Qiao, Q.; Zhao, M.; Yin, W.; Mao, D.; Zhang, H.; Xu, Z. A *Chem. Commun.* **2014**, *50* (99), 15811–15814.
- (6) Sk, B.; Khodia, S.; Patra, A., *Chem. Commun.* **2018**, *54* (14), 1786–1789.
- (7) Haidekker, M. A.; Theodorakis, E. A., *Org. Biomol. Chem.* **2007**, *5* (11), 1669–1678.
- (8) Fischer, D.; Theodorakis, E. A.; Haidekker, M. A., *Nat. Protoc.* **2007**, *2* (1), 227–236.
- (9) Suhling, K.; French, P. M. W.; Phillips, D., *Photochem. Photobiol. Sci.* **2005**, *4* (1), 13–22.
- (10) Peng, X.; Yang, Z.; Wang, J.; Fan, J.; He, Y.; Song, F.; Wang, B.; Sun, S.; Qu, J.; Qi, J.; et al. *J. Am. Chem. Soc.* **2011**, *133* (17), 6626–6635.
- (11) Cao, J.; Wu, T.; Hu, C.; Liu, T.; Sun, W.; Fan, J.; Peng, X., *Phys. Chem. Chem. Phys.* **2012**, *14* (39), 13702–13708.
- (12) Hu, R.; Lager, E.; Liu, J.; Lam, J. W. Y.; Sung, H. H. Y.; Williams, I. D.; Zhong, Y.; Wong, K. S., *J. Phys. Chem. C* **2009**, 15845–15853.
- (13) Sengupta, S.; Pandey, U. K., *Org. Biomol. Chem.* **2018**, *16* (12), 2033–2038.
- (14) Li, J.; Qian, Y.; Xie, L.; Yi, Y.; Li, W.; Huang, W., *J. Phys. Chem. C* **2015**, *119* (4), 2133–2141.

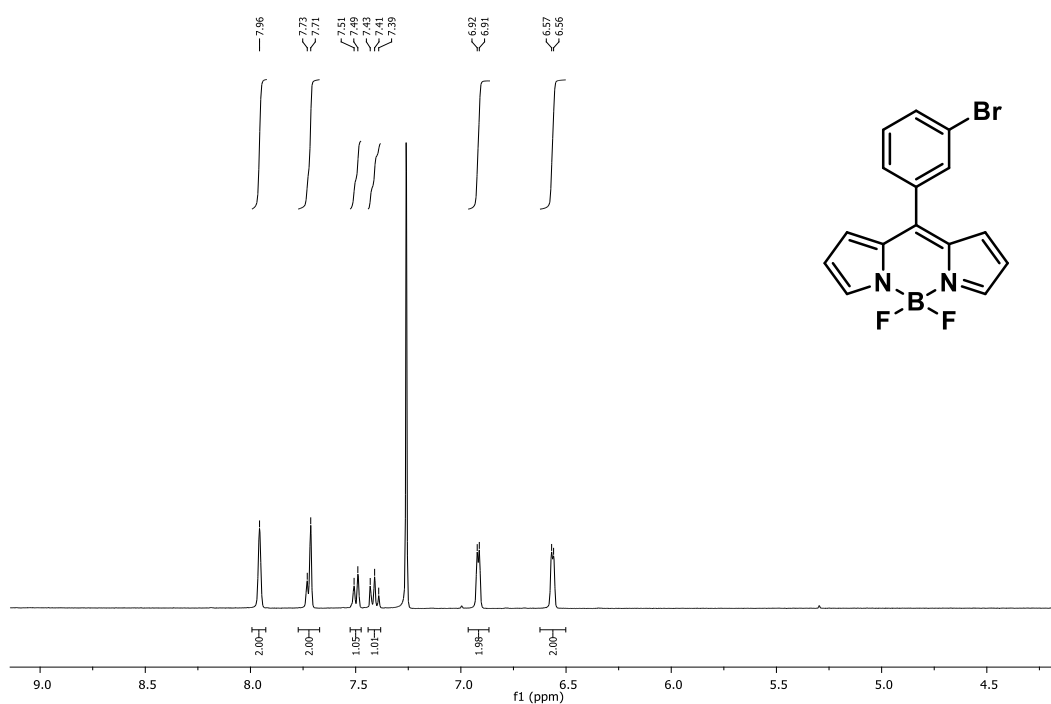
- (15) Tarafdar, G.; Sengupta, S.; Pandey, U. K.; Ramamurthy, P. C., *2017 IEEE 44th Photovolt. Spec. Conf. PVSC 2017* **2018**, 1–6.
- (16) Chen, D.; Zhong, C.; Zhao, Y.; Liu, Y.; Qin, J., *Mater. Chem. Front.* **2017**, *1* (10), 2085–2093.
- (17) Kim, H. G.; Jo, S. B.; Shim, C.; Lee, J.; Shin, J.; Cho, E. C.; Ihn, S. G.; Choi, Y. S.; Kim, Y.; Cho, K., *J. Mater. Chem.* **2012**, *22* (34), 17709–17717.
- (18) Albano, G.; Lissia, M.; Pescitelli, G.; Aronica, L. A.; Di Bari, L., *Mater. Chem. Front.* **2017**, *1* (10), 2047–2056.
- (19) Ge, G.; Gu, J.; Yu, J.; Zhu, E.; Hai, J.; Bian, L.; Zhang, F.; Xu, Z.; Ma, W.; Tang, W., *Phys. Chem. Chem. Phys.* **2015**, *17* (12), 7848–7856.

## APPENDIX

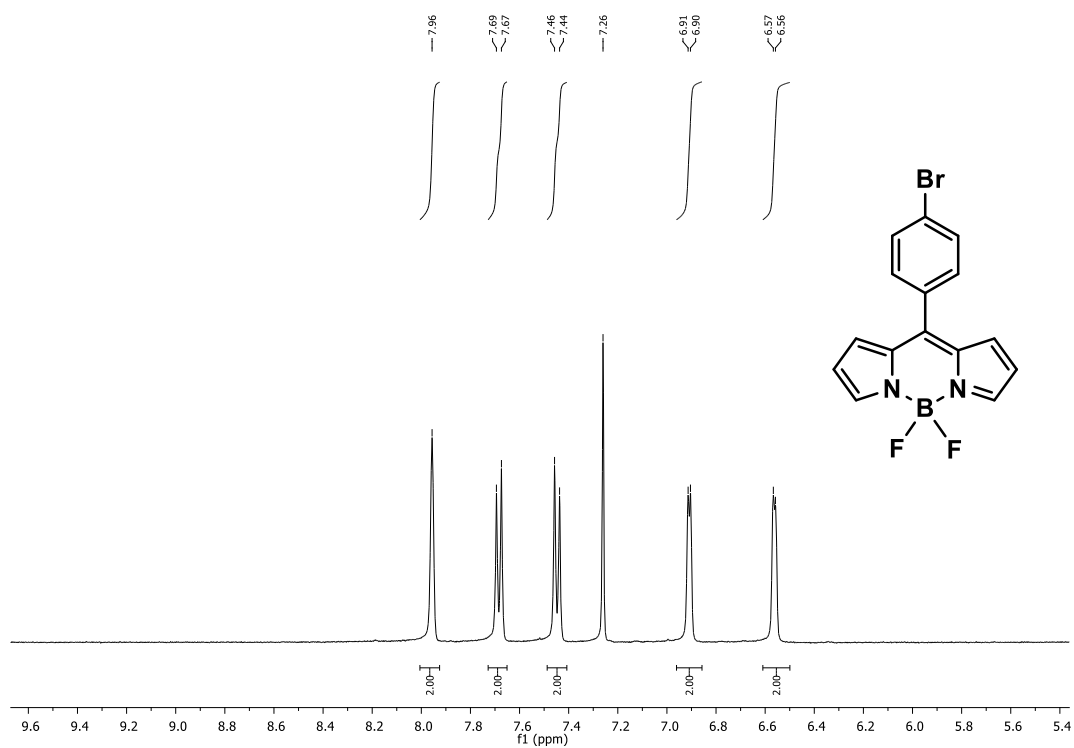
### 2,2'-((3-bromophenyl)methylene)bis(1H-pyrrole), (2), $^1\text{H}$ NMR, $\text{CDCl}_3$ , 400 MHz



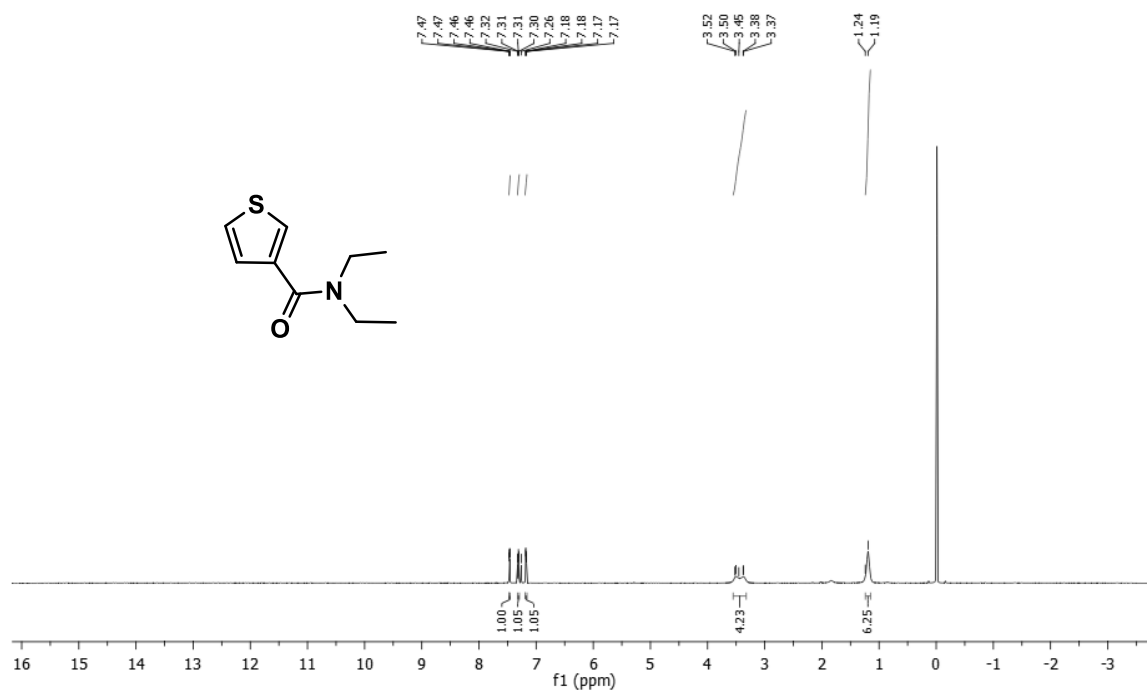
### Acceptor m-BODIPY-Br, (3), $^1\text{H}$ NMR, $\text{CDCl}_3$ , 400 MHz



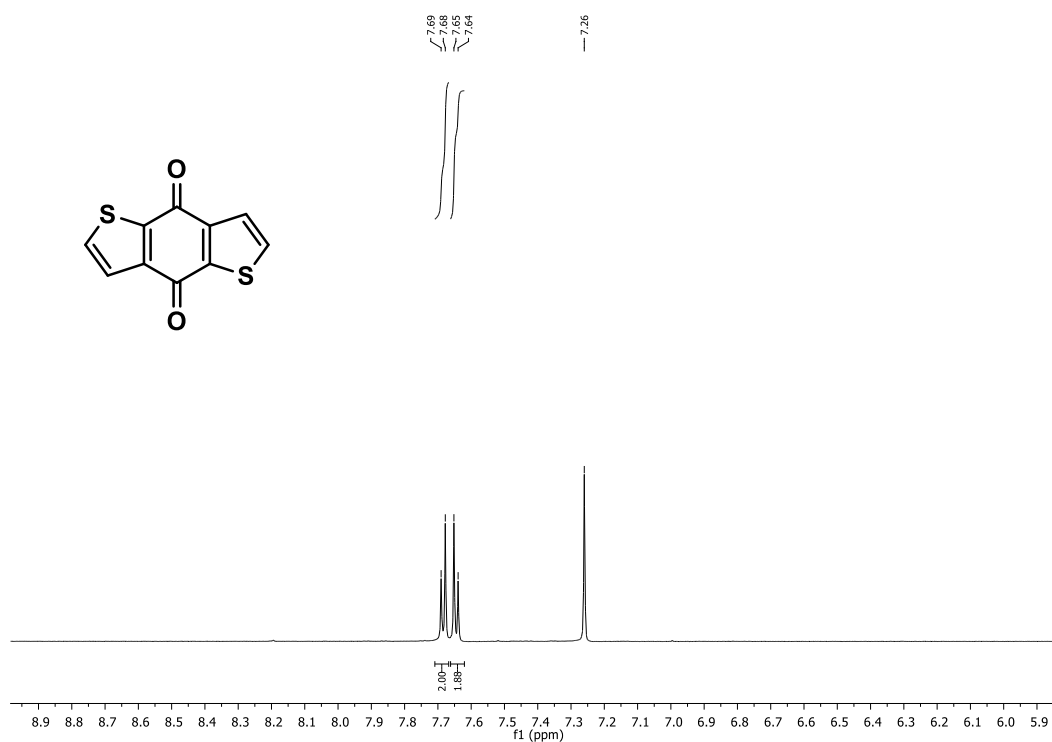
Acceptor p-BODIPY-Br, (5),  $^1\text{H}$  NMR,  $\text{CDCl}_3$ , 400 MHz



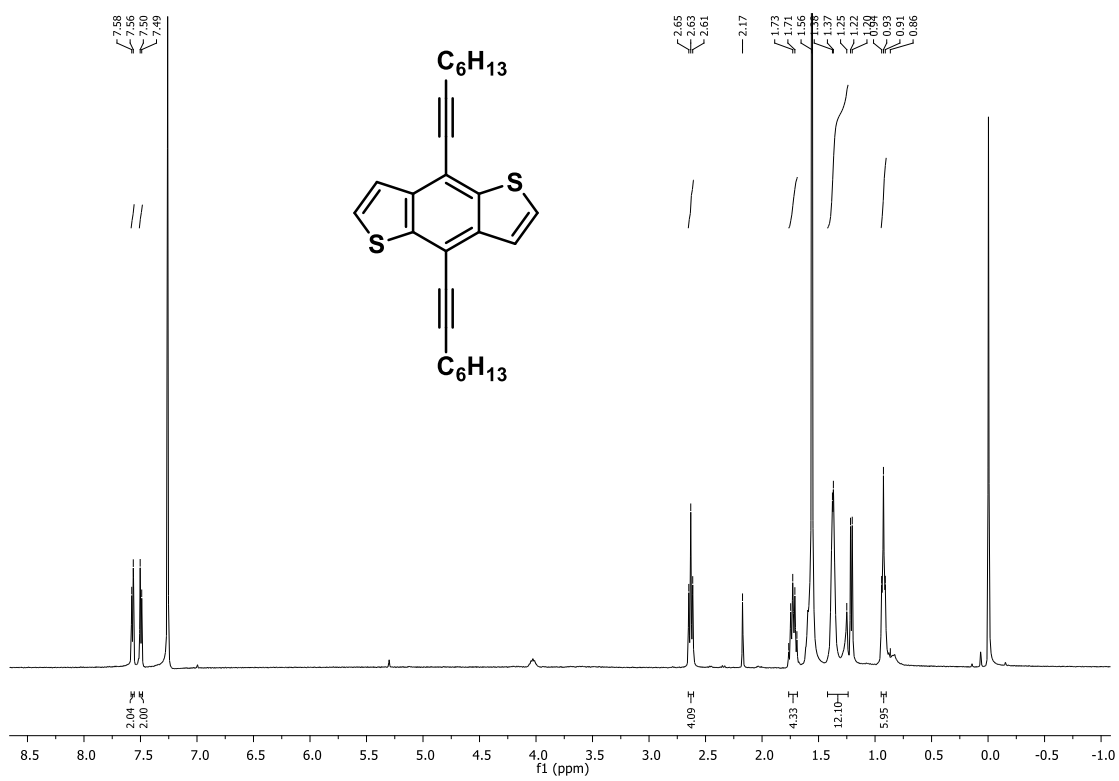
(*N,N*-diethyl)thiophenecarboxamide, (7),  $^1\text{H}$  NMR,  $\text{CDCl}_3$ , 400 MHz



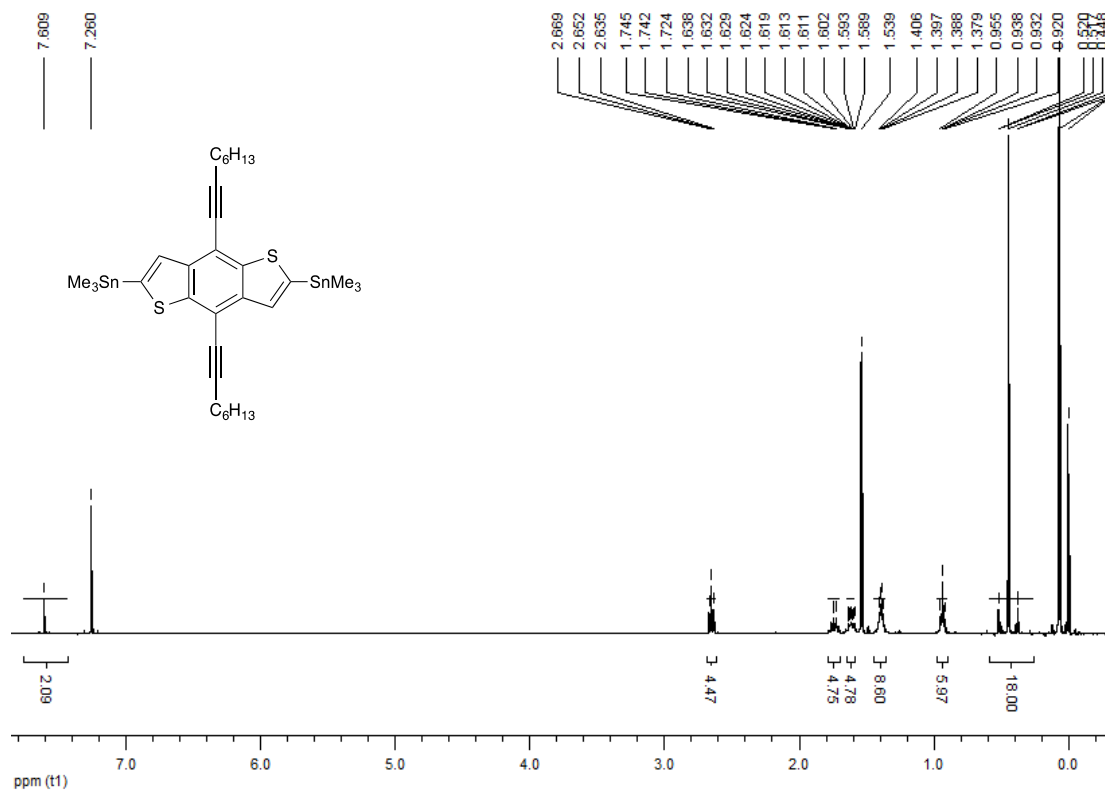
**Benzo[1,2-b:4,5-b']dithiophene-4,8-dione, (8),  $^1\text{H}$  NMR,  $\text{CDCl}_3$ , 400 MHz**



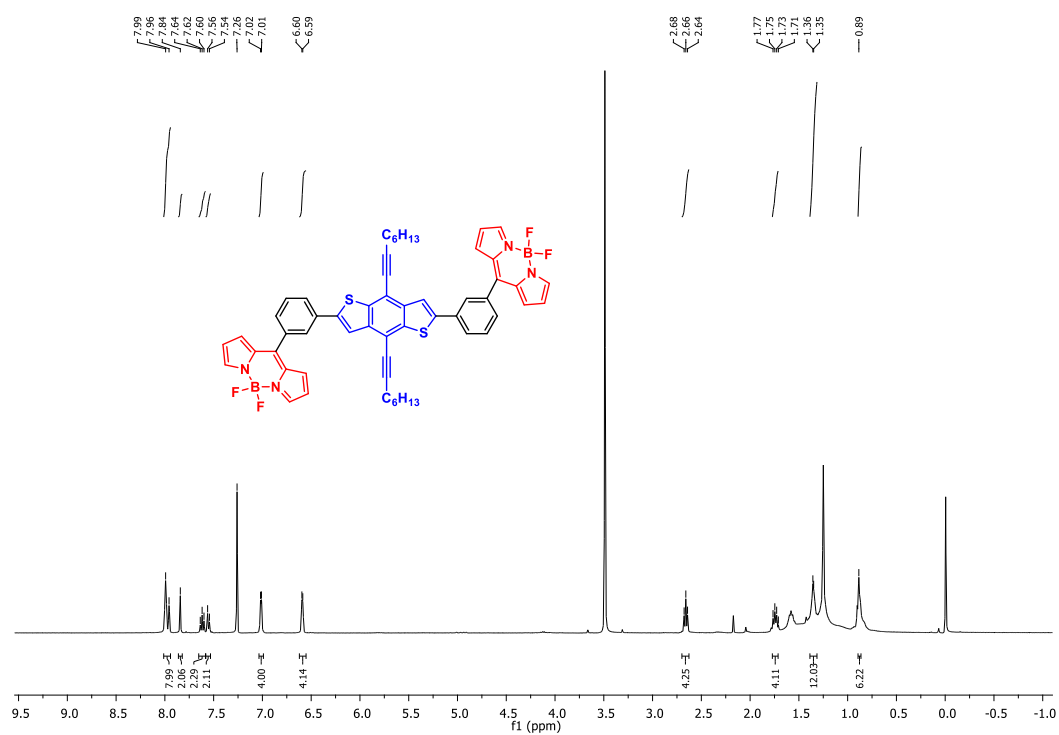
**4,8-Di(oct-1-yn-1-yl)benzo[1,2-b:4,5-b']dithiophene, (9),  $^1\text{H}$  NMR,  $\text{CDCl}_3$ , 400 MHz**



(4,8-di(oct-1-yn-1-yl)benzo[1,2-b:4,5-b']dithiophene-2,6-diyl) bis(trimethylstannane), (10),  $^1\text{H}$  NMR,  $\text{CDCl}_3$ , 400 MHz

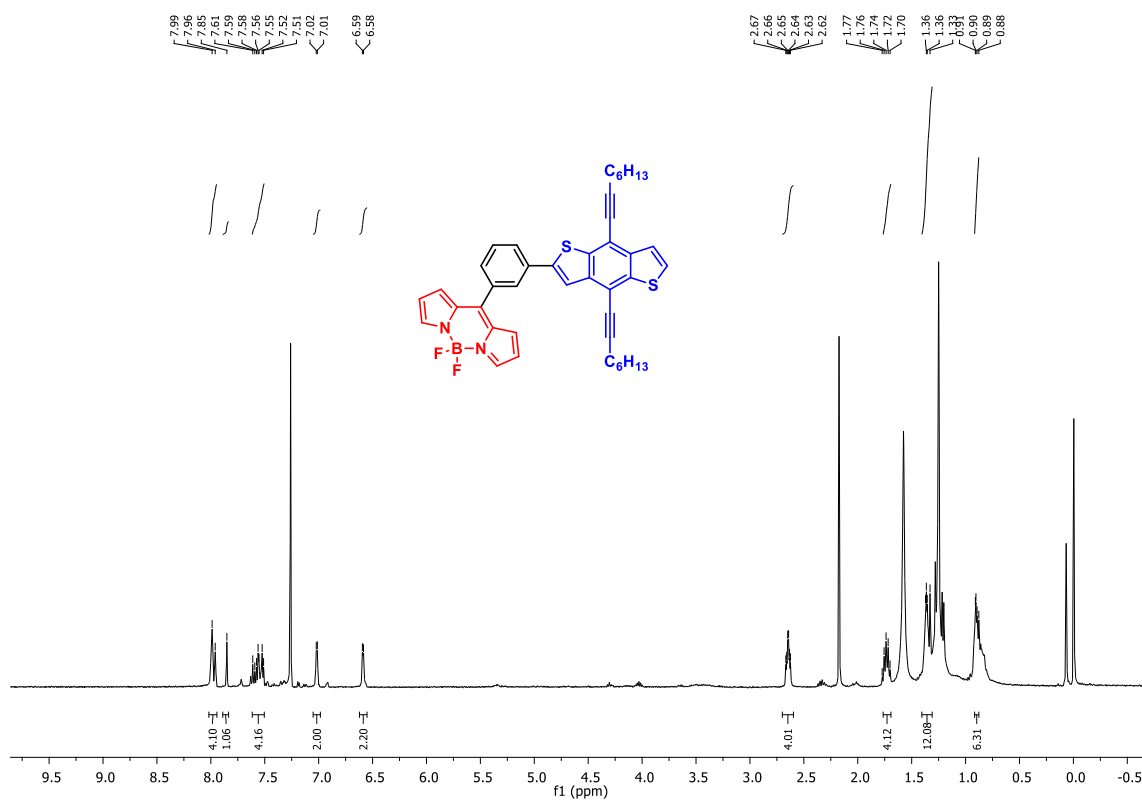


m-ADA triad, (11),  $^1\text{H}$  NMR,  $\text{CDCl}_3$ , 400 MHz

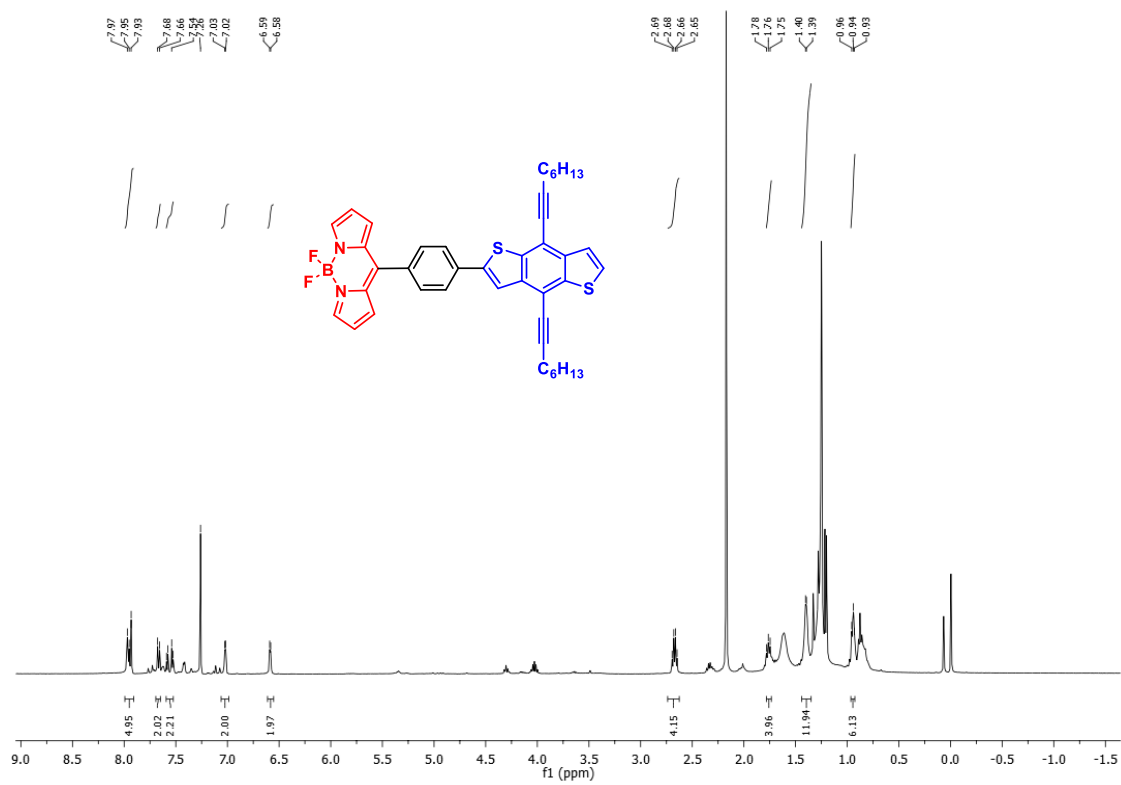




**m-AD dyad, (12),  $^1\text{H}$  NMR,  $\text{CDCl}_3$ , 400 MHz**

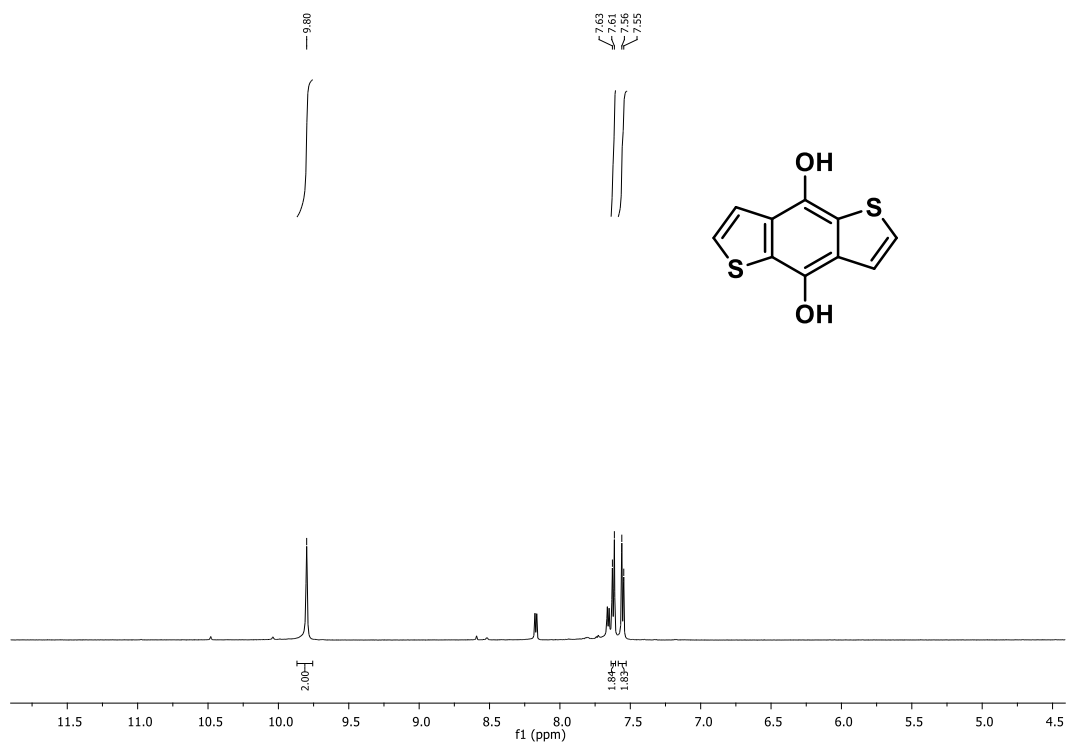


**p-AD dyad, (13),  $^1\text{H}$  NMR,  $\text{CDCl}_3$ , 400 MHz**





4,8-Dihydroxybenzo[1,2-b:4,5-b']dithiophene, (15),  $^1\text{H}$  NMR, DMSO, 400 MHz



4,8-Bis(trifluoromethanesulfonyloxy)benzo[1,2-b:4,5-b']dithiophene, (16),  $^1\text{H}$  NMR,  $\text{CDCl}_3$ , 400 MHz

